Age-Specific Study of Airflow Distribution, Aerosol Transport and Deposition in an Unhealthy Human Lung using CFD-DPM Approach

Author

HAFIZ HAMZA RIAZ

Regn Number

NUST-2021-MSME-00000360883

Supervisor

Dr. ADNAN MUNIR

DEPARTMENT OF MECHANICAL ENGINEERING

SCHOOL OF MECHANICAL & MANUFACTURING ENGINEERING

NATIONAL UNIVERSITY OF SCIENCES AND TECHNOLOGY

ISLAMABAD

JUNE 23, 2023

Age-Specific Study of Airflow Distribution, Aerosol Transport and Deposition in an Unhealthy Human Lung using CFD-DPM Approach
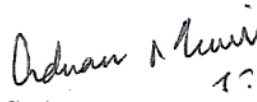
Author

HAFIZ HAMZA RIAZ

Regn Number

NUST-2021-MSME-00000360883

A thesis submitted in partial fulfillment of the requirements for the degree of

MS Mechanical Engineering

Thesis Supervisor:

Dr. ADNAN MUNIR

Thesis Supervisor's Signature: _____

DEPARTMENT OF MECHANICAL ENGINEERING

SCHOOL OF MECHANICAL & MANUFACTURING ENGINEERING

NATIONAL UNIVERSITY OF SCIENCES AND TECHNOLOGY,

ISLAMABAD

JUNE 23, 2023

MASTER THESIS WORK

We hereby recommend that the dissertation prepared under our supervision by: **Hafiz Hamza Riaz (2021-MSME-360883)**

Titled: **Age-specific study of airflow distribution, aerosol transport and deposition in an unhealthy human lung using CFD-DPM approach**

be accepted in partial fulfillment of the requirements for the award of degree.
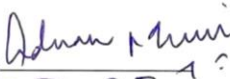
Examination Committee Members

1. Name: Dr. Emad Uddin   Signature: _____

2. Name: Dr. Zaib Ali   Signature: _____

Supervisor's name: Dr. Adnan Munir   Signature: _____

Date: 3-7-23

_____
Head of Department   Date: 3-7-23

COUNTERSINGED

Dean/Principal

Date: 3-7-23

Thesis Acceptance Certificate

Certified that final copy of MS thesis written by _Hafiz Hamza Riaz_ Registration No. _2021-MSME-360883_, of SMME has been vetted by undersigned, found complete in all respects as per NUST Statutes / Regulations, is free of plagiarism, errors, and mistakes and is accepted as partial fulfillment for award of MS degree. It is further certified that necessary amendments as pointed out by GEC members of the scholar have also been incorporated in the said thesis.

Signature: _____

Name of Supervisor: _Dr. Adnan Munir_

Date: _23/06/23_

Signature (HOD): _____

Date: _26/6/23_

Signature (Principal): _____

Date: _3-7-23_

iii

Certificate for Plagiarism

It is certified that MS Thesis Titled: **Age-Specific Study of Airflow Distribution, Aerosol Transport and Deposition in an Unhealthy Human Lung using CFD-DPM Approach** by **Hafiz Hamza Riaz** (**NUST-2021-MSME-00000360883**) has been examined by me. I undertake the follows:

a. Thesis has significant new work/knowledge as compared already published or are under consideration to be published elsewhere. No sentence, equation, diagram, table, paragraph, or section has been copied verbatim from previous work unless it is placed under quotation marks and duly referenced.

b. The work presented is original and own work of the author (i.e., there is no plagiarism). No ideas, processes, results, or words of others have been presented as Author own work.

c. There is no fabrication of data or results which have been compiled/analyzed.

d. There is no falsification by manipulating research materials, equipment, or processes, or changing or omitting data or results such that the research is not accurately represented in the research record.

e. The thesis has been checked using TURNITIN (copy of originality report attached) and found within limits as per HEC plagiarism Policy and instructions issued from time to time.
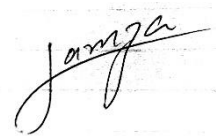
Name & Signature of Supervisor

Dr. ADNAN MUNIR

Signature**:**_____

i

Declaration

I certify that this research work titled "*Age-Specific Study of Airflow Distribution, Aerosol Transport and Deposition in an Unhealthy Human Lung using CFD-DPM Approach*" is my own work. The work has not been presented elsewhere for assessment. The material that has been used from other sources it has been properly acknowledged / referred.

HAFIZ HAMZA RIAZ

NUST-2021-MSME-00000360883

Copyright Statement

Acknowledgements

Dedicated to my exceptional parents and adored siblings whose tremendous support and cooperation led me to this wonderful accomplishment.

Abstract

The pulmonary route is the pathway to transport aerosolised drug particles into the tracheobronchial airways to treat and prevent respiratory diseases. Lung cancer is a frequently diagnosed respiratory disease caused by particulate matter in the environment, especially among older individuals. It is evident that as age increases, the lung airway diameters reduce, and this geometric alteration due to aging affects the breathing capacity, transportation, and deposition (TD) of inhaled drugs. A precise understanding of the inhaled particles TD through age-specific unhealthy respiratory tracts containing a tumor can potentially optimise lung cancer treatment, especially among aged individuals, which has not been investigated in the existing literature. This study investigates the aging effect on the deposition of inhaled drug particles on the glomus tumor present in the upper airways of the human respiratory tract. The CFD model predicts that particle deposition on the tumor wall is higher in the 70-year-old lung for the particle sizes ranging from 5-10 μm, while the maximum deposition efficiency of 10-20 μm particles is found in the lung of a 50-year-old individual. The results of the numerical study show that particle sizes ranging from 10-14 μm are deposited with higher efficiency on the tumor wall as compared to the smaller size particles (5-9 μm) for 50, 60 and, 70 age. The flow disturbances are found maximum in the airway downstream of the tumor. Furthermore, the effect of different inhalation flow rates on particles (TD) is also investigated. The obtained patterns of airflow distribution and deposition efficiency on the tumor wall and in the upper tracheobronchial airways would be beneficial for developing an efficient and targeted drug delivery system.

Keywords: *Tumor, Aging Effect, Pulmonary Disease, Drug Delivery, Environmental Exposure, Fluid-Particle Interaction*

Table of Contents

List of Figures

List of Tables

CHAPTER 1

INTRODUCTION

Environmental exposure, mutations, and particulate matter in polluted air are factors associated with lung cancer [2, 3]. Cigarette smoke (active and passive) is the leading cause of lung cancer and is responsible for around 90% of lung cancer deaths [4]. These environmental factors lead to glomus tumor which is a rare growth that comes from glomus cells and looks a bit like a smooth muscle [5]. The unrestricted growth of these cells in the respiratory regions makes up a lump of mass which is termed a lung tumor or cancer. Lung cancer was the leading cause of cancer death by 2020 and currently, it is the second most diagnosed cancer with an estimated 2.2 million new cases and 1.8 million deaths. It contributes around 11.4 % of the total cancers diagnosed and responsible for 1 in 5 (18%) cancer-related deaths [6]. The presence of a tumor in the respiratory airways partially blocks the airflow path and affects the breathing capacity of a person. Drug aerosol intake in the human respiratory tract through inhaling devices like dry powder inhaler (DPI) or nebuliser is an effective means of treating lung diseases and other respiratory illnesses [1, 7]. Moreover, inhaling medicinal drugs has negligible risk of adverse side effects which are associated with the traditional drug delivery methods [8]. However, the particulate matter present in the environment, such as those found in traffic, smoke, and dust, can move in a similar manner as medicinal drugs in the respiratory tract, posing potential health risks [9]. Hence, adequate deposition of medicinal aerosols to the targeted areas of unhealthy respiratory airways like a tumor surface or swollen region is crucial for prompt healing. Figure 1 provides a comprehensive illustration of various aspects of lung tumors, including their growth stages, the environmental factors that contribute to their development, the global incidence of lung cancer relative to other types of cancer, commonly used inhalation devices for treating tumor cells, and how the geometrical dimensions of the human lung change with age.
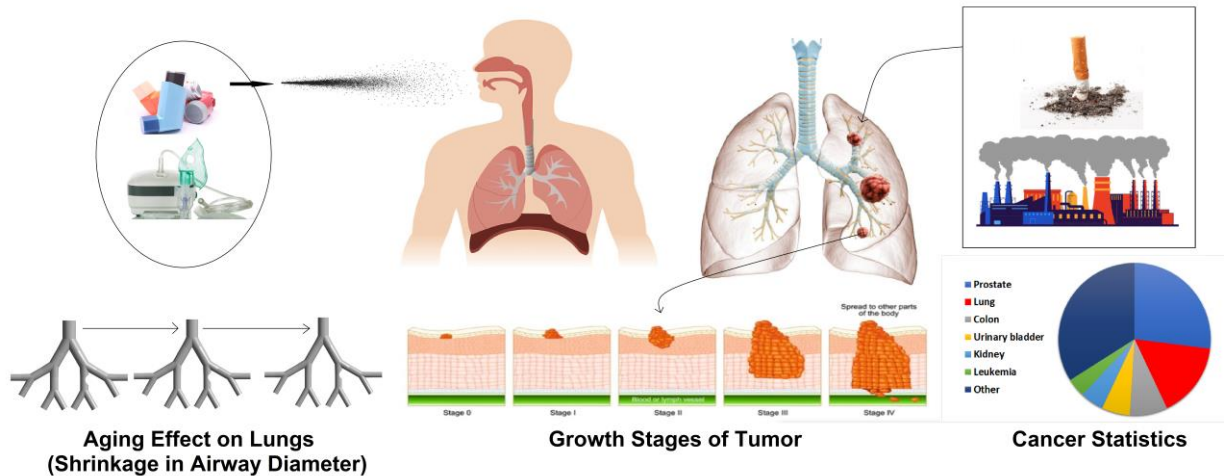
Figure 1: A general depiction of aging effect on lungs, cancer statistics and application of inhaled drugs for treating the tumor cells in lungs.

1.1 Literature Review

Multiple cases have been studied and presented in the literature dealing with the growth and resection of glomus tumors found in the human respiratory tract. Parker, et al. [10] conducted a case study on the restriction of airflow due to intrathoracic airway obstruction in which a glomus tumor of polypoid shape was found in the portion of the distal trachea of a 43-year-old woman. Similarly, there are multiple cases reported relating the growth of tumors such as the growth and resection of a 2 cm^3 glomus tumor covered by normal mucosa in the lungs of a 70-year-old man [11]; two different cases of growth and resection of glomus mass in the lower tracheal region [12]; and the growth of a polypoid tumor in the trachea [13], etc.

Engineers and scientists in the field of biomedical engineering have employed computational fluid dynamics (CFD) to study the airflow, transportation, and deposition (TD) of medicinal aerosols and particulate matter in polluted air through the complex pathways of the human respiratory system [9, 14-23]. Many studies have been conducted on healthy and ideal lung model which is a symmetric 3D lung geometry based on the dimensional parameters provided by Weibel, et al. [24]. The deposition efficiency of injected aerosol particles in the lungs changes with age considerably especially for the age range of children, teenagers, and old age [25]. Xu and Yu [26] studied the aerosol deposition in the respiratory models of ages ranging from children to adults. They found that deposition efficiency in the mouth-throat region was higher

for small age as compared to the adults whereas the opposite was true for the alveolar and pulmonary region [27]. Patterson, et al. [28] reported a study on the deposition of nano-size particles in the respiratory model of subjects belonging from age of eight to eighteen years. The numerical results demonstrated that the trapping of particles in the bronchial region for children was higher than in teenagers. When comparing teenagers with adults, it was found that particles get deposited more easily in the respiratory tract of teenagers as their lung models were smaller in size [29].
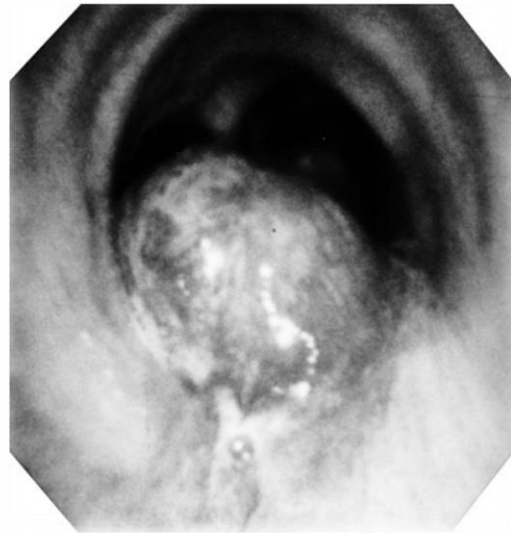
Figure 2: Growth of a polypoid tumor in the tracheal region of human lung, reported by [13]

Flow behaviour and deposition of particles at micron size in the oropharynx were examined by Huang and Zhang [30]. They reported that impact mechanism played a significant role in the trapping of particles, especially at bifurcation junctions. Rahman, et al. [25] studied the deposition of aerosols in the age-specific ideal lung models and found that the deposition fraction increased with age in the upper airways. Also, they observed that particles with a size equal to or greater than 20 microns deposited nearly 100% in generations G0-G5, with no particles traversing G7. Whereas about half of the smaller-sized particles ended up depositing in the lower respiratory airways, specifically beyond G14. This motivates the use of size for the injected particles up to 20 microns in the present study which comprises lung generations G3-G6.

The number of numerical studies conducted on unhealthy lungs in comparison to healthy lungs is less in the existing literature. CFD can assist researchers in understanding the flow

physics of unhealthy lungs and how environmental aerosols affect them for better treatment of pulmonary diseases. Segal, et al. [31] performed numerical simulations to study the growth of the side wall tumor on the carinal ridge in the respiratory airways of a 4-year-old patient. They found that the carinal ridge tumor has significant effect on the flow patterns and the flow downstream of the tumor. Based on the evaluation of respiratory flow, Yang, et al. [32] reported that the presence of any obstructive medium in the airways has direct effects on the airflow velocity streamlines. They also performed detailed comparison of the airflow behaviour and wall shear stress under various ventilatory settings and in both healthy and unhealthy lungs.. Sul, et al. [33] generated lung models with no obstructions and with symmetric and random obstructions. They demonstrated a significant difference between the flow patterns in healthy and unhealthy lungs, more so during the expiratory flow as compared to the inhalation phase.

All these studies focused on the variations of airflow patterns but only few have investigated the behaviour of drug deposition in an obstructed or unhealthy airway tract. Martonen and Guan [34] investigated the effects of size of lung tumors on the airflow patterns and the influence of particle diameter on the transportation and deposition rate in the respiratory pathways. Particles of three different sizes (0.21, 3.50, 7.24 μm) were injected, and it was found that small particles were deposited less on the tumor surface compared to larger particles due to weak impact mechanism. Additionally, when the tumor size ratio (r/R) was varied from 0 to 2, it was observed that localised flow patterns were dominant for tumors with a size ratio of 0.8 or less [35]. Kleinstreuer and Zhang [1] numerically investigated the existence of single and double hemispherical side wall tumors in the 5th generation of an ideal respiratory tract model. They found that the tumor size and location have substantial influence on the deposition fraction of inhaled drugs. Around 11% of particles deposited on the tumor surface for critical tumor radius *r/R*=1.25 with the constant inhalation flow rate of 60 liter per minute. Luo, et al. [36] examined the behaviour of aerosol transport in an unhealthy lung suffering from a chronic obstructive pulmonary disease which causes inflammation and narrowing of airways just like a tumor. Their findings showed that the deposition fraction of particles is significantly influenced downstream of the obstructive pathway. Srivastav, et al. [37] examined the effect of a polypoid tumor on the behaviour of wall shear stress. They reported high flow disturbances around and downstream of the tumor. Similar findings were reported by Singh [38] in a study on the effect of presence of a glomus tumor in the trachea on the airflow streamlines, secondary flows, and particle deposition.

1.2   Research Motivation

Growth of glomus tumors in the respiratory tract is an uncommon disease, but it can occur between the age group of children to adults and in various locations of the respiratory tract such as the trachea, major lobes, and main airway branches [11, 39-41]. Studying the impact of tumors on airflow and particle deposition in bronchial airways can be beneficial for environmental dosimetry and health effect studies, as well as for analyzing drug-aerosol delivery. Singh [38] and Srivastav, et al. [37] performed simulations on unhealthy respiratory models which included glomus tumors in the trachea region of the lung. Kleinstreuer and Zhang [1] studied the effect of the location and size of a hemispherical tumor in the 5th generation of the lung model on the particle deposition on tumor surfaces. However, they did not study the age-specific particle deposition as well as the effect of a broad particle size range on the deposition efficiency in the upper airways of the unhealthy respiratory tract. The global incidence of lung cancer is increasing, with diagnosis often occurring around the age of 70 [42]. Hence, it is essential to have a clear understanding of drug particle deposition in the respiratory tracts of aged individuals, to facilitate optimised treatment of the disease.

1.3   Research Objective

The objective of this study is to numerically investigate the impact of a glomus hemispherical tumor in the upper airways of the age-specific lungs on the transport and deposition of micro-scale particles. To achieve this objective, 3D ideal lung models with symmetric and planar pathways from G3-G6 are generated for ages 50, 60, and 70 years. G3-G6 section is used to simulate the effects of upper airway tumors[1, 43]. Additionally, this approach neglects the cartilaginous rings present in the larynx, trachea (G0), and main bronchi (G1). The study analyses in detail the airflow distribution and particle deposition on the tumor surface for each age-specific lung model and compares them using 3D numerical simulations. The effect of particle size and inlet airflow rate on deposition efficiency is studied. The study aims to provide a detailed understanding of the effect of reduction in airway sizes as a result of aging on the TD of the inhaled drug on the tumor surface in age-specific lung.

CHAPTER 2

NUMERICAL METHODOLOGY

2.1   Lung Geometry

Three-dimensional lung models from generation three to six are generated for ages 50, 60, and 70 years. According to the designed models used by Xu and Yu [26], the geometric parameters of the age-specific lung models used in this study are listed in table 1. The variations in the geometrical parameters for an adult lung are very negligible from the age of 30 to 50 [44]. Consequently, it was assumed that a lung at the age of 30 is comparable to a lung at the age of 50. From 50 years old onward, the airway diameters for each generation shrink by 10% after every 10 years [45] and the tissues of the lung become 7% hardened especially between the ages of 50 to 80 [46]. The lung models for three adults are constructed using the parameters listed in table 1.

Table 1: Geometric parameters of lung model used by Xu and Yu [26]

Generation Number	Airway Diameter (mm)			Airway Length (mm)
	50 year	60 year	70 year	
3	5.60	5.04	4.48	7.59
4	4.50	4.05	3.60	12.68
5	3.50	3.15	2.80	10.71
6	2.80	2.52	2.24	9.01
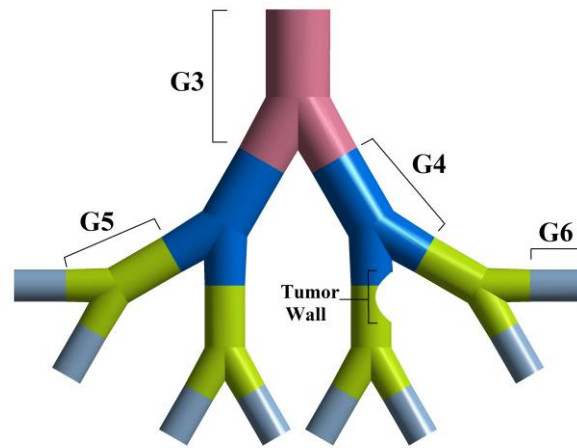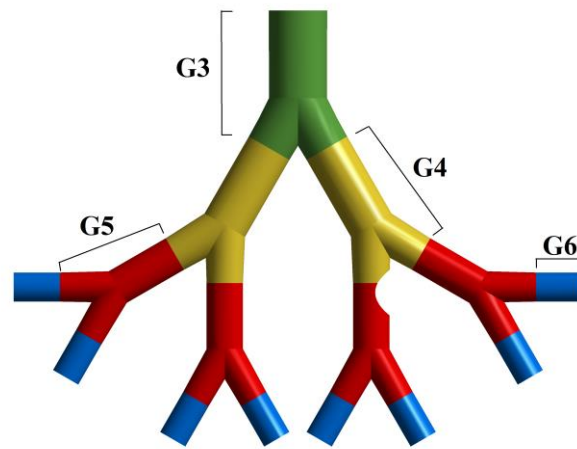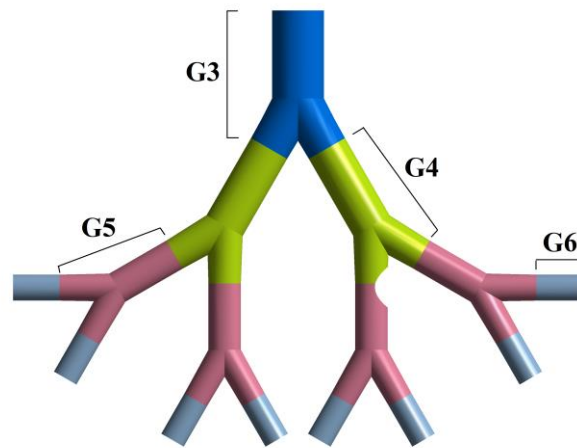
Figure 3: Tracheobronchial lung airway models (G3-G6) with sidewall tumor for the 50 (a), 60 (b) and 70 (c) year-old lung.

Figure 3 shows the lung models with a tumor in the 5th generation for each age group. The airway length of each generation remains constant, but its diameter reduces with the increase of the age. Only four generations are simulated because studying the complete lung model demands unaffordable computational time. An effective cutting method is employed to create a sidewall hemispherical glomus tumor in G5 of each lung model. The location selected for the sidewall tumor corresponds to the published data available in the literature [1, 31, 47]. Moreover, the location of the tumor is also appropriate in the sense that it does not impact the aerosol distribution and profiles of the inlet air velocity at 3rd generation. The blockage of the tumor to the airflow in the airway can increase from 20% at mild stage to 80% at late stage [48]. Exposure to environmental pollutants increases the risk of lung cancer and affects the size of the tumor [49]. The radius (r) of the hemispherical tumor on the airway wall is selected based on the radius of the local pathway (R) in which the tumor is present and is defined by the ratio r/R. Using the geometrical parameters listed in table 1 and choosing the ratio for the tumor size as r/R= 1.25 which corresponds to around 50% blockage of the airway [1], the lung models for each age are modelled on SolidWorks and are demonstrated in Figure 3.

2.2   Numerical Model

The simulations are conducted using the ANSYS Fluent software. For the airflow in airways, the governing equations are:

$$\frac{\partial \rho}{\partial t} + \frac{\partial}{\partial x_1}(\rho u_1) = 0 \tag{1}$$

$$\frac{\partial}{\partial t}(\rho u_1) + \frac{\partial}{\partial x_2}(\rho u_1 u_2) = -\frac{\partial p}{\partial x_1} + \frac{\partial}{\partial x_2}\left[\mu\left(\frac{\partial u_1}{\partial x_2} + \frac{\partial u_2}{\partial x_1}\right)\right] \\ + \frac{\partial}{\partial x_2}(-\rho u_1' u_2') \tag{2}$$

where ρ is the density of the air which is 1.225 kg/m^3, μ is the dynamic viscosity taken as 1.79×10^{-5} kg/m.s., p is the pressure of air, $\vec{u}_1$ and $\vec{u}_2$ are the fluid velocity in the horizontal and vertical direction, respectively, x_1 and x_2 represent the horizontal and vertical direction in the fluid, respectively. The Shear-Stress Transport (SST) $k - \omega$ turbulence model is used to simulate the turbulence as it is proved to be more suitable for the adverse pressure gradients [50]. The SST $k - \omega$ model is a modification of the standard $k - \omega$ model to efficiently incorporate

8

the robust and correct formulation in the near-wall sections with the free-stream independence in the far-field section.

The SST $k - \omega$ turbulence model integrated with the essential blending functions is given in the following equations:

$$\frac{\partial}{\partial t}(\rho k) + \frac{\partial}{\partial x_1}(\rho k u_1) = \frac{\partial}{\partial x_2}\left(\Gamma_k \frac{\partial k}{\partial x_2}\right) + \tilde{G}_k - Y_k + S_k, \tag{3}$$

$$\frac{\partial}{\partial t}(\rho \omega) + \frac{\partial}{\partial x_1}(\rho \omega u_1) = \frac{\partial}{\partial x_2}\left(\Gamma_\omega \frac{\partial \omega}{\partial x_2}\right) + \tilde{G}_\omega - Y_\omega + D_\omega + S_\omega. \tag{4}$$

Γ_k and Γ_ω represents the effective diffusivity of turbulent kinetic energy (k) and dissipation rate (ω) respectively in equation 3 and 4. $\tilde{G}_k$ represents the generation of turbulence kinetic energy (k) and $\tilde{G}_\omega$ represents the generation of specific dissipation rate (ω). Y_k and Y_ω represents the dissipation of turbulent kinetic energy and dissipation rate respectively. D_ω is the cross-diffusion term and S represents the respective source term. This model has proved to generate satisfactory results, resolving the high-pressure gradient flows near the wall, and predicting accurate outputs at the boundary layer [51-54].

For the interpolation of the diffusion and pressure gradients, the least squares cell-based technique is employed. The employed approach involves utilizing a pressure-velocity coupling scheme, in addition to implementing a second-order upwind scheme for the turbulent kinetic energy, specific dissipation rate, and momentum. Moreover, a second-order implicit scheme is used to solve the numerical equations. A constant inlet velocity and pressure outlet boundary conditions are employed for each lung model [55, 56]. The required inlet air velocity during the inhalation phase is calculated depending upon the size of the inlet surface of G3. For the turbulence, the specification method used is intensity and viscosity ratio with values of turbulent intensity and turbulent viscosity ratio as 5% and 10 respectively. A constant velocity is used instead of an unsteady velocity inlet profile to examine the impact of the aging effect on the deposition of particles on the tumor without the influence of variations in the velocity. In the lung model, the wall is assumed to be stationary, and a no-slip condition is imposed on the wall surfaces.

The present model uses one-way coupling between the primary and discrete phases which focuses only on the particle motion in airflow and ignores any kind of influence on the airflow by the particles. The choice of coupling depends upon the concentration of the secondary phase

(particle) in the primary phase (air). For all the drug delivery applications, the disperse phase concentration is well below 15% which allows the use of one-way coupling instead of a two-way coupling model [57]. In the numerical simulations, the interaction between particles can be disregarded since the particle suspension injected into the inlet of the lung airway model is sufficiently dilute. [58].

In this study, the Discrete Phase Model (DPM) is utilized to capture the interaction between the discrete and continuous phases. The Lagrangian approach is employed to simulate the transport and dispersion of particles within the lung airways. The motion and behavior of each particle are governed by the force balance equation:

$$\frac{d\vec{u}_p}{dt} = F_D(\vec{u} - \vec{u}_p) + \frac{\vec{g}}{\rho_p}(\rho_p - \rho)$$

(5)

where u and u_p represents the velocity of continuous and discrete phase respectively, g is the gravitational acceleration, ρ_p is particle density which is taken as 1100 kg/m^3 [25, 59].

$F_D(\vec{u} - \vec{u}_p)$ represents the drag force and the F_D is determined using the following relation:

$$F_D = \frac{18\mu}{\rho_p d_p^2} C_D \frac{\text{Re}_P}{24}$$

(6)

where C_D represents drag coefficient, d_p denotes diameter of the particle and Re_p is the particle Reynolds number defined as:

$$\text{Re}_p = \frac{\rho d_p |u_p - u|}{\mu}$$

(7)

To account for particle deposition, a trap condition is imposed on the lung model's wall. Additionally, an escape condition is applied at all airway outlets, specifically at the exit point corresponding to generation six. [60, 61]. This ensures that when a particle strikes the inner region of the airway, the fate of that particle will be considered trapped or deposited at that point of the airway. Effect of different inhalation flow rates has also been studied on the particle TD. Velocities corresponding to different inlet flow rates are listed in Table 2. It has been found that aging is linked with a continuous decrement in the inhalation parameters including tidal volume and breathing rate. Table 3 lists the breathing frequencies and tidal volume for different ages.

Table 2: Inlet velocities (m/s) for three ages and flow rates

Flow Rate (l/m)	50 Year	60 Year	70 Year
60	5.075	6.265	7.929
45	3.806	4.699	5.947
30	2.537	3.132	3.964

Table 3: Inhalation parameters for three 50, 60 and 70 year *[44]*

Parameter	50 Year	60 Year	70 Year
Breathing Frequency (min^{-1})	13.65	13.19	12.92
Tidal Volume (ml)	500	403	179

The deposition efficiency for any region is defined as the ratio of a number of particles trapped in the targeted region to the total number of particles injected at the inlet surface. Equation 8 shows the expression used for calculating deposition efficiency in this study. In the numerical simulations, 30,000 spherical particles [1] with a constant particle size were injected randomly from the inlet face of the lung section.

$$Deposition\ Efficiency = \frac{\text{Number of particles trapped in the targeted region}}{\text{Total number of particles injected at the inlet}} \times 100 \qquad (8)$$

2.3   Mesh Dependency Study

The mesh dependency study is carried out by performing multiple numerical simulations of the 50-year-old lung model with generations G3-G6 at inlet flow rate of 60 liter/min using the injected particle diameter as 7 µm. A total of six meshes were constructed with same structural properties but different mesh densities. The tetrahedral element number of the meshes ranged from 286,966 in Mesh 1 to 1,016,872 in Mesh 6. The changes in the deposition efficiency of particles on the lung wall of G3 with a varying number of meshed elements are shown in Figure 4. The deposition efficiency maintains almost a constant value after Mesh 4 with 689,804 elements. Mesh 5 with 761,052 tetrahedral elements is selected for all the numerical simulations and analysis. Figure 5 demonstrates the mesh at the inlet section of G3. A total of 10 layers of inflation are used near the wall for the accurate prediction of the flow of the wall surface inside the lung model. The mesh at the bifurcation of G3 and mesh density near the tumor wall is also demonstrated and the mesh structure of each of the six meshes is the same as the one illustrated in Figure 5.
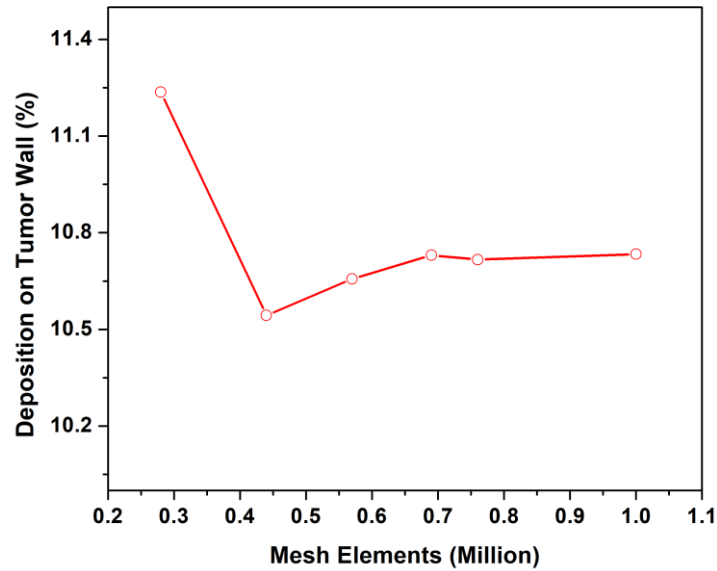
Figure 4: Variation of deposition efficiency at tumor wall as function of the number of elements of the 50-year lung model, particle diameter of 7µm and inlet flow rate of 60 liter/min.
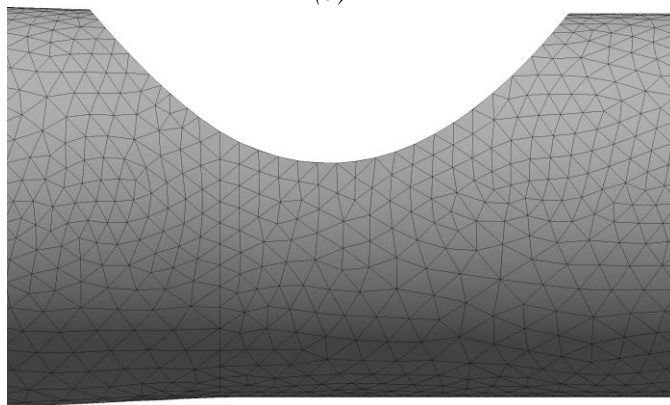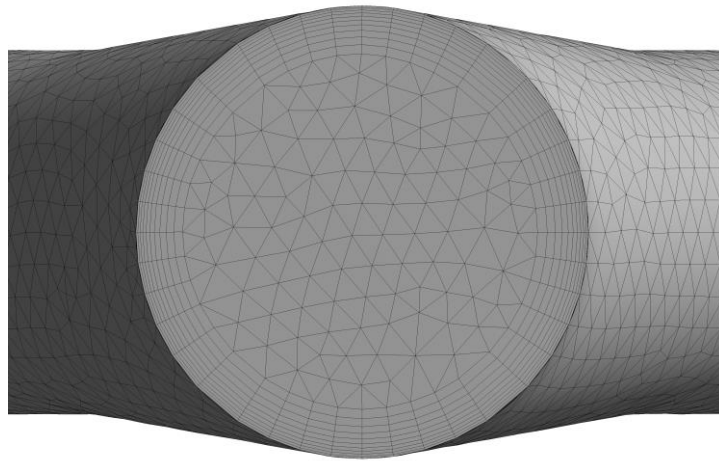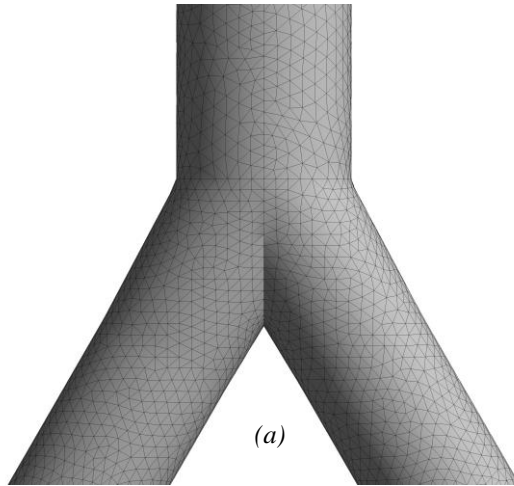
Figure 5: Computational mesh for the lung model. The mesh quality on the lung wall (a); Inflation layers at the inlet wall (b); Mesh density near tumor wall (c).

2.4   Validation of Model

In the present study, the numerical model is validated by comparing its results with published experimental and numerical data concerning particle deposition in the lung section spanning from generation three to generation six (G3-G6) [62-64]. Various particle diameters ranging from 3µm to 7µm and flow rate of 60 liter/min for the 50-year-old healthy lung model are used for conducting simulations and the results from the current model are found to be in good proximity with the experimental and numerical results at different Stokes numbers as demonstrated in Figure 6. The Stokes number (Stk) is a dimensionless parameter that characterizes the interaction between a particle and a fluid flow. It is defined as the ratio of the particle's response time (the time it takes for the particle to react to the fluid forces) to the characteristic time scale of the fluid flow [65]:

$$Stk = \frac{\rho_p d_p^2 u}{18\mu D} \qquad (9)$$
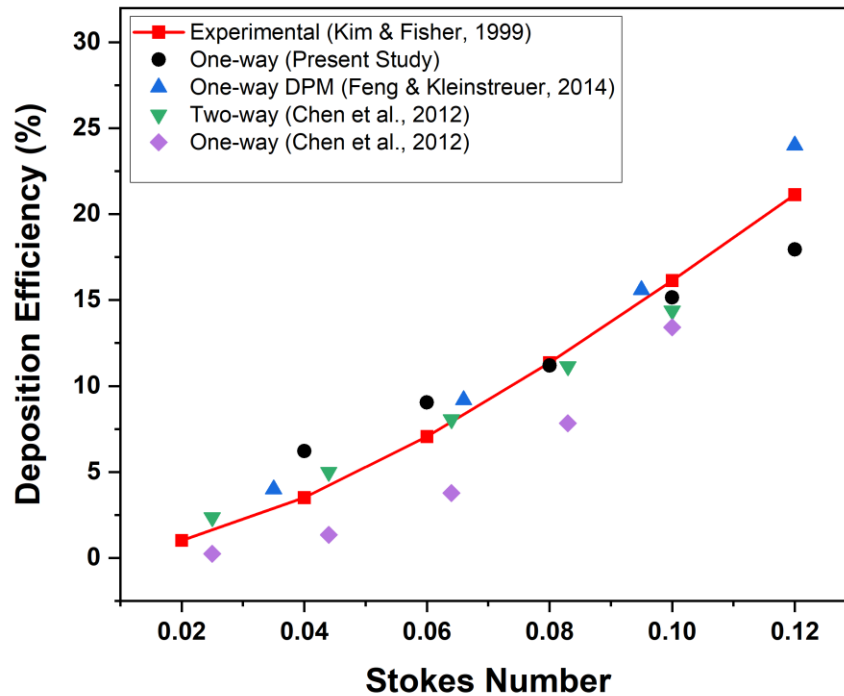
Figure 6: Comparison of the deposition efficiencies obtained for the first bifurcation of the G3-G6 lung model at various Stokes number between the present study and published experimental and numerical results *[62-64]*

14

where D represents the airway diameter of the inlet of G3 through which the particles are being injected and u is the mean inlet velocity of the air. Moreover, the comparison of the present deposition efficiency on the tumor wall for r/R=0.2, 0.6, 1.0, 1.25 and 1.5 with the numerical results reported by Kleinstreuer and Zhang [1] is shown in Figure 7. The obtained trend lines of deposition efficiency against tumor sizes in the present study demonstrate a strong agreement with the published data. This agreement serves as evidence that the current numerical model is accurate in calculating particle transport and deposition in the tracheobronchial airways of the lung.
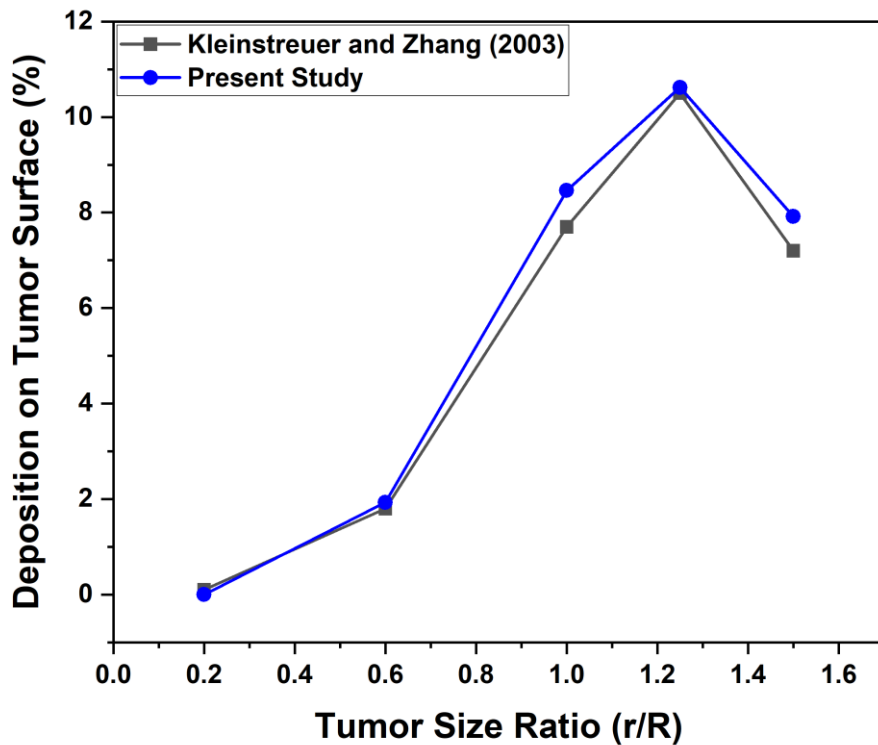
Figure 7: Comparison of results of deposition efficiency at tumor wall in the 5th generation obtained from the present study and literature [1].

CHAPTER 3

RESEARCH AND DISCUSSION

The simulations are performed for each lung model using an inlet flow rate of 60 liter/min and eight particle diameters ranging from 5 µm-20 µm. The effect of various inhalation conditions are investigated by conducting the simulations using three inlet flow rates: 60 liter/min, 45 liter/min, and 30 liter/min, which represent heavy, moderate, and light breathing conditions respectively for the 50-year-old lung model [37].

3.1   Airflow Distribution

The air velocity and wall shear stress contours for G3-G6 lung models of three ages are illustrated in Figure 8 and 9 respectively for the inlet flow rate of 60 liter/min. The contours show that velocity reduces as the flow moves into deeper generations because the total cross-sectional area of the airways increases. The velocity in the 70-year-old lung model is highest owing to its smallest diameter as compared to the other ages. The variation in velocity and wall shear at every bifurcation area is significant, and a trend of increased velocity and shear stress is found as the air passes through the bifurcation point. From the velocity contours in Figure 8, a non-uniform distribution of velocity as the flow passes the first and second bifurcation is found. As the air reaches the bifurcating point of the airways, its velocity skews towards the inner wall of the airway and reduces towards the outer wall. This is due to the separation of the streamlines owing to geometrical deflections at the bifurcation regions of the airways and the generation of secondary vortices as shown in Figure 10. The obtained pattern of velocity distribution matches the pattern reported in the literature .

Moreover, the velocity and wall shear stress on the tumor increases with the increase of age. The impact mechanism observed in the study reveals that there is a greater deposition of particles on the tumor wall and at the bifurcation point in the 70-year-old model. Conversely, the 50-year-old model exhibits a lower number of particles deposited in comparison. The impact mechanism
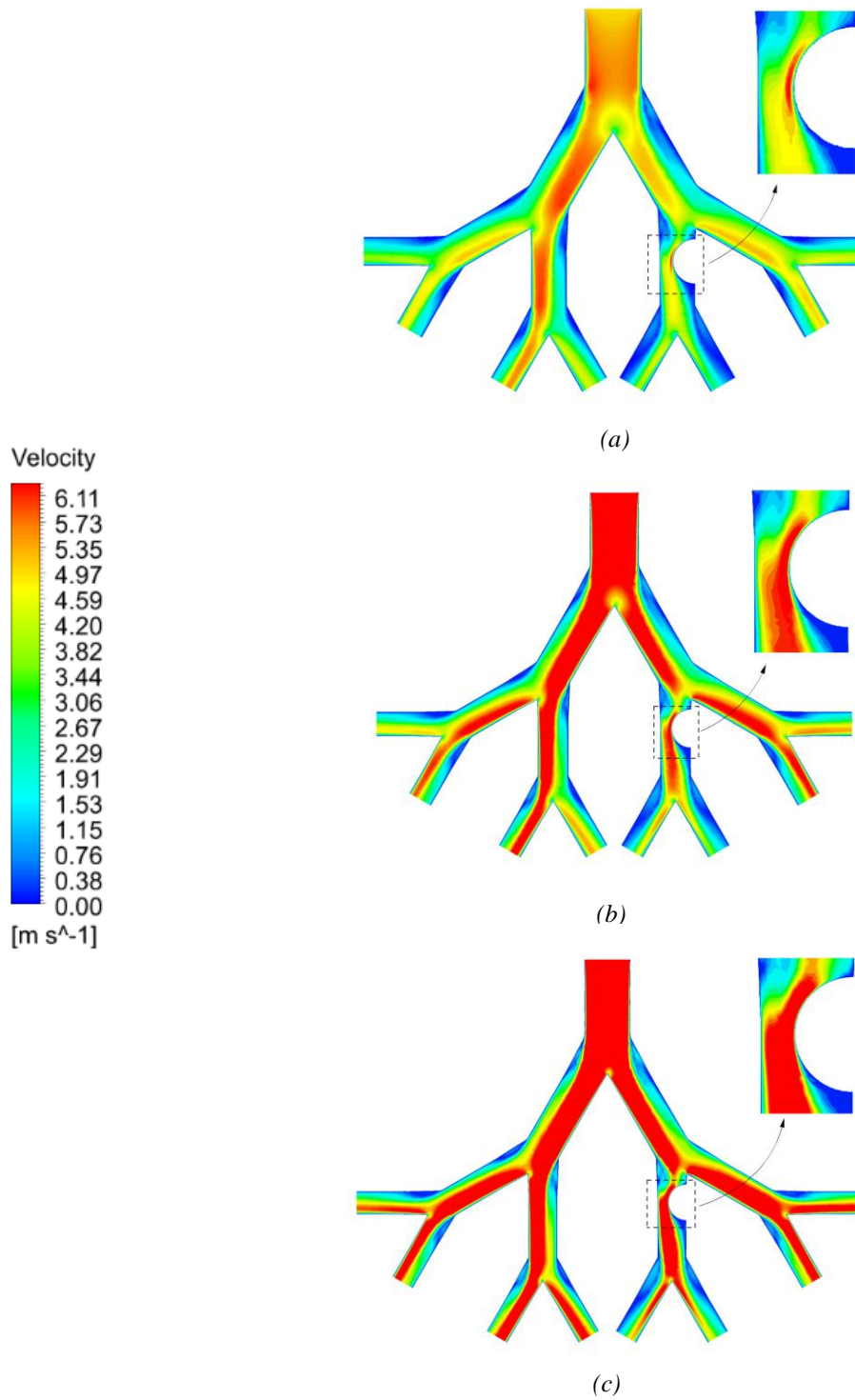
Figure 8: Airflow velocity contours for age 50 years (a), 60 years (b) and 70 years (c) old model at 60 liter/min.

involves particles colliding with surfaces due to their inertia and is affected by both flow velocity and particle size. Higher flow velocities result in greater momentum exchange, while smaller particles are more likely to follow the fluid flow and larger particles are more likely to collide with surfaces. The momentum exchange between particles and surfaces is influenced by particle mass and velocity, making particle size and flow velocity important factors in determining the impact mechanism and resulting particle deposition. A higher flow velocity in the 70-year-old model ensures higher impact mechanism. The velocity and wall shear contours obtained for the flow rates of 45 liter/min and 30 liter/min follow the same trend as shown in Figure 8 and 9 respectively but with small magnitudes.

Figure 11 illustrates the relationship between pressure drop and various inlet flow rates for each age group. It is observed that the maximum pressure drop occurs in the narrow airways of the 70-year-old lung model. At a flow rate of 60 liters/min, it is observed that the pressure drop in the 70-year-old lung model increases by 58.82% compared to the 50-year-old model. This indicates that breathing is more difficult for a 70-year-old patient than for younger patients.

Figure 12 displays the pressure contours for the three age groups at an inlet flow rate of 60 liters/min. As the flow progresses into the deeper airways, the magnitude of pressure diminishes. As shown in Figure 8, a high velocity in the 70-year-old lung requires a high-pressure gradient to move the flow at the inlet. High pressure is found in the airway located before the unhealthy generation for all ages. This is because most of the flow gets skewed towards the left branch of the lung as it passes through the bifurcation point, leaving the right branch with low velocity and hence high pressure. Moreover, the magnitude of the pressure is found to be negative as the flow passes the constriction region. The narrow airway due to the tumor causes the air velocity to increase significantly, and as a result, the pressure in this region decreases.

The velocity contours at the different cross-sectional planes defined in Figure 13a are shown in Figure 13b. These planes include those near the airway with a tumor and those near the airway at the same generation without a tumor. The flow originates from the inlet surface of the third generation (G3) and proceeds towards the first bifurcation point, where it then splits into two main branches. However, the right branch of the lung model is partially blocked in G5.4 by the tumor, causing a constricted side in comparison to the left branch. This results in the flow being skewed more towards the left branch (G4.1) of the lung model based on the continuity principle,

Figure 9: Wall Shear contours for age 50 years (a), 60 years (b) and 70 years (c) old model at the flow rate of 60 liter/min.

Figure 10: Separation of streamlines and generation of secondary vortices on the symmetric plane at the bifurcation region of G3.
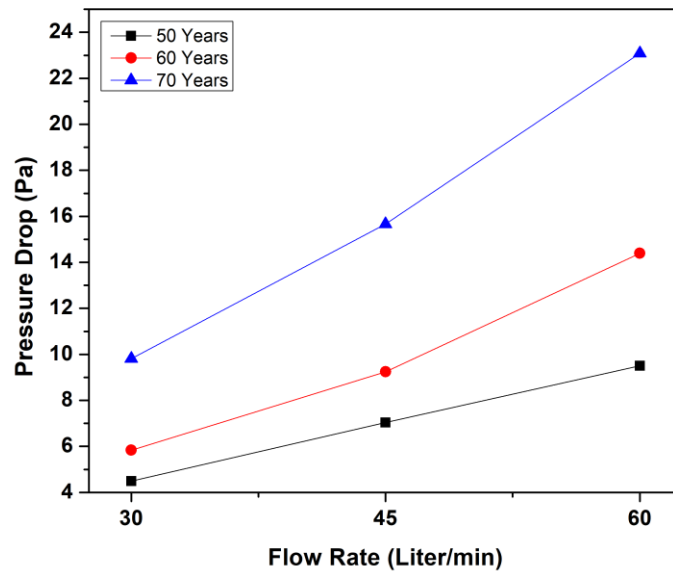
Figure 11: Pressure Drop at different inlet flow rates for 50-, 60- and 70-year-old lung.

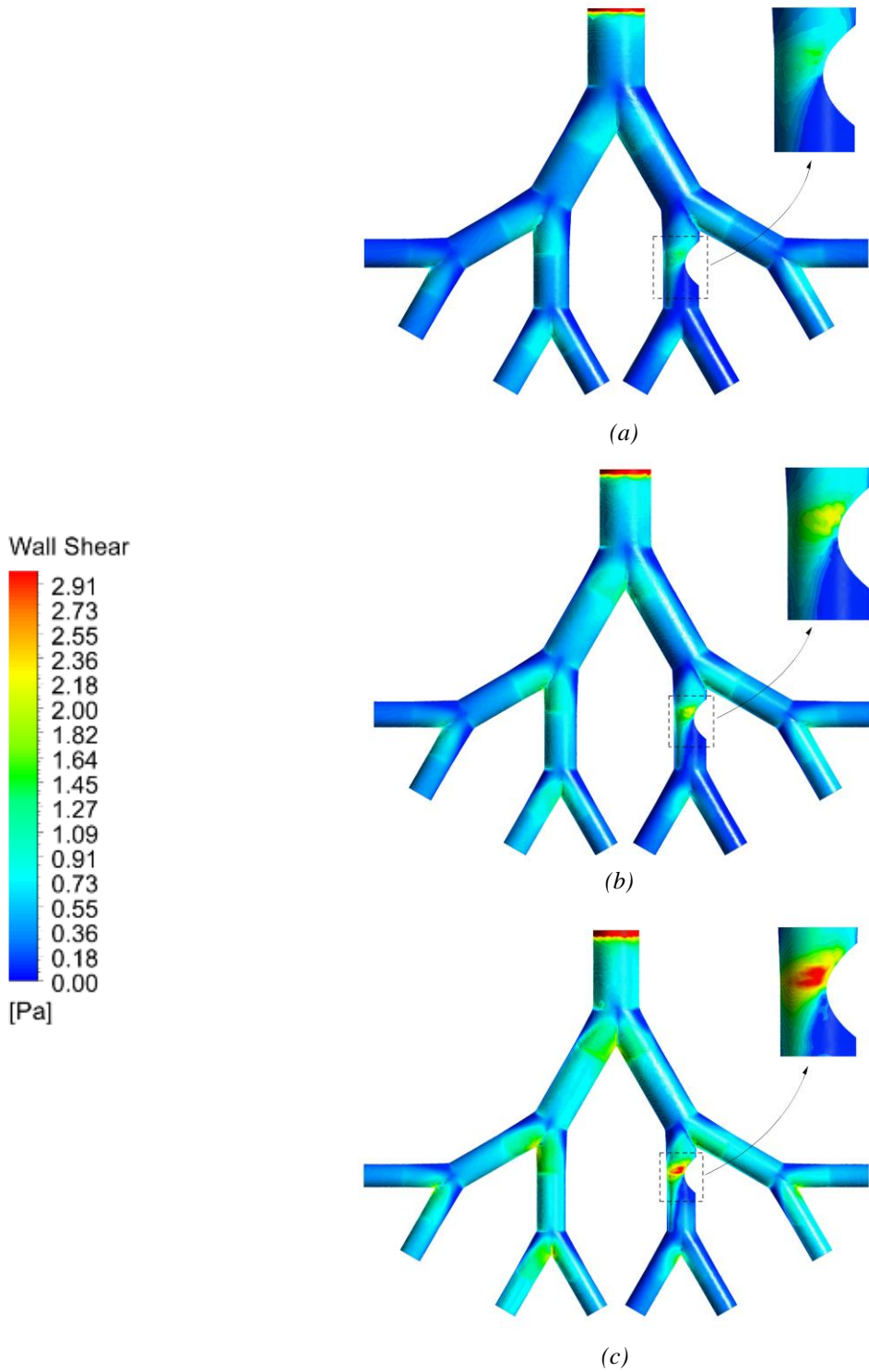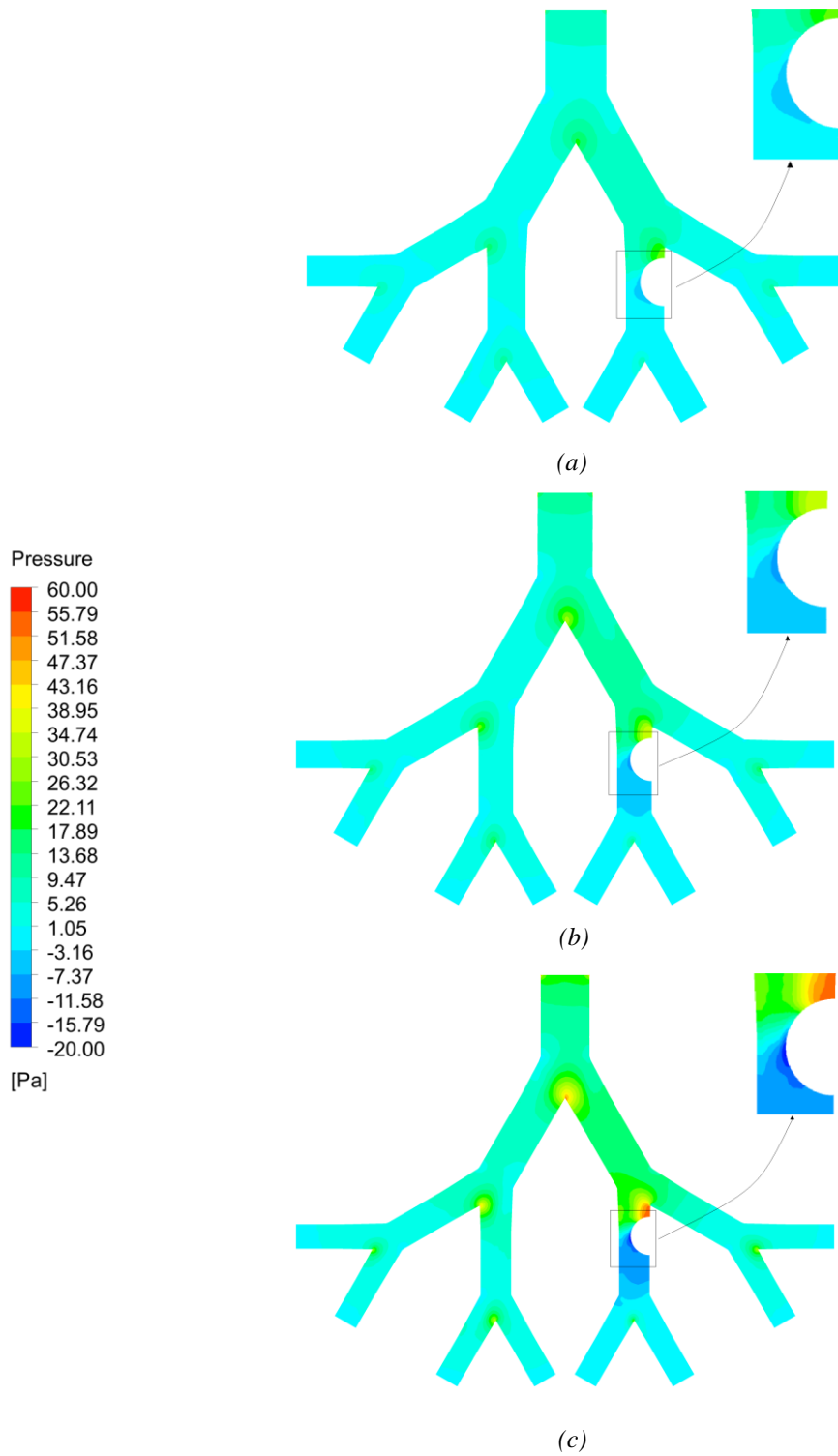**Figure 12:** Pressure contours for age 50 years (a), 60 years (b) and 70 years (c) old model at the flow rate of 60 liter/min.

generating high-velocity contours in the healthy airway as compared to the unhealthy airway with the presence of a tumor.

Additionally, the airway blockage by the tumor hinders the smooth inhalation of respiratory airflow resulting in aerosol deposition. From Figure 13b, the velocity distribution upstream of the tumor is almost symmetric as compared to the healthy lung without tumor. The reduction of airway sectional area (blockage) caused by the tumor increases the velocity at the center-plane (B´-B) of the tumor surface and its downstream. The peak velocity is observed in the 70-year-old lung because the maximum shrinkage of the lung generations and the airflow patterns have considerable effects on downstream of the tumor as compared to the upstream. Also, the magnitudes of velocity in G5.2 with no tumor are higher especially for the downstream plane when compared with the magnitudes of velocity in G5.4 with the presence of a tumor.

Figure 14 illustrates the velocity distributions at horizontal lines located at the center of cross-sectional planes of each lung model at the flow rate of 60 liter/min. The velocity gradient increases continuously as the age increases. Velocity distribution for line B-B' is maximum because of the reduced cross-sectional area of the airway due to the presence of the tumor. It is interesting to observe that the velocity distribution remains almost symmetric along the line A-A´; whereas, for the line C-C´, the airflow velocity is skewed towards the inside of the airway as is also found from Figure 13b. For the healthy generation, the velocity profile remains almost identical along the airway as indicated by the profiles of three lines D-D´, E-E´, and F-F´ in Figure 14.

Figure 15 displays the contours of turbulence energy across various cross-sectional planes located in the healthy and unhealthy airways at the flow rate of 60 liter/min. The turbulence kinetic energy amplifies with age as the diameter of the airways narrows and flow velocity surges. Additionally, the highest level of turbulence kinetic energy occurs at the cross-sectional plane situated at the tumor's center (B´-B) in all age models. The tumor causes disturbances in the airflow pattern within the airways, resulting in fluctuations during the inhalation process, ultimately leading to a heightened turbulence energy at the central plane. When comparing the age models, maximum turbulence energy is found in the 70-year lung model because of a high velocity gradient and low airway diameters.
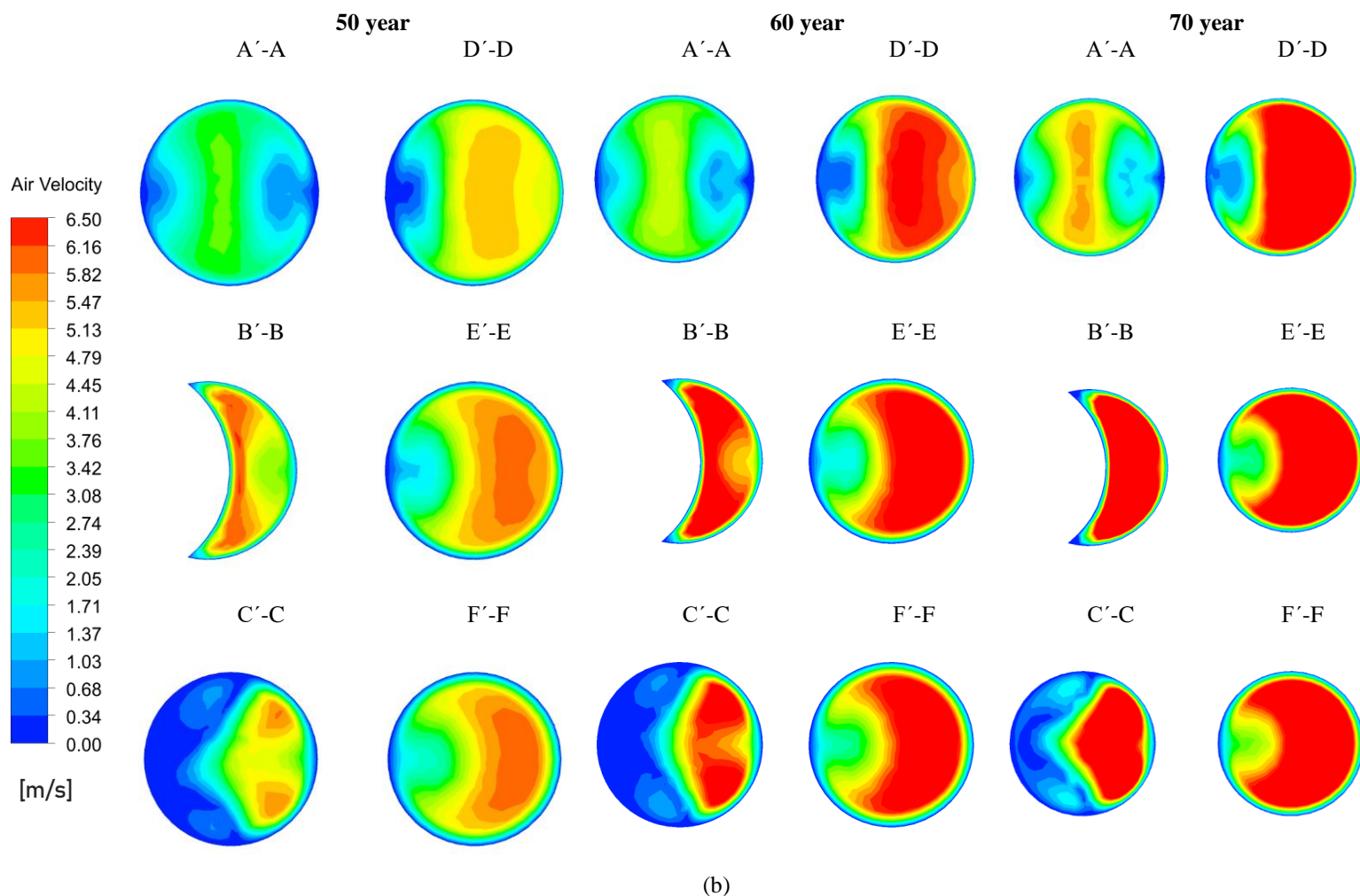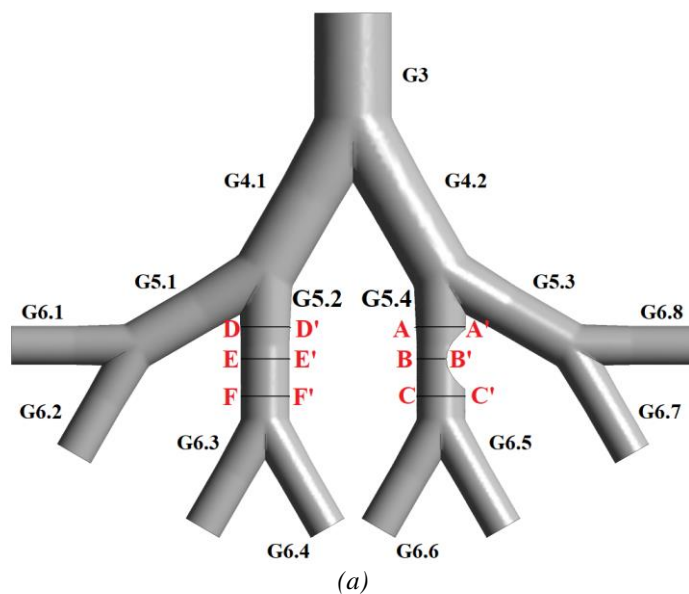
Figure 13: Location of cross-sectional planes in a lung model (a) and Velocity contours at the different cross-sectional planes of 50-, 60-, and 70-year-old lung model for flow rate of 60 liter/min (b).
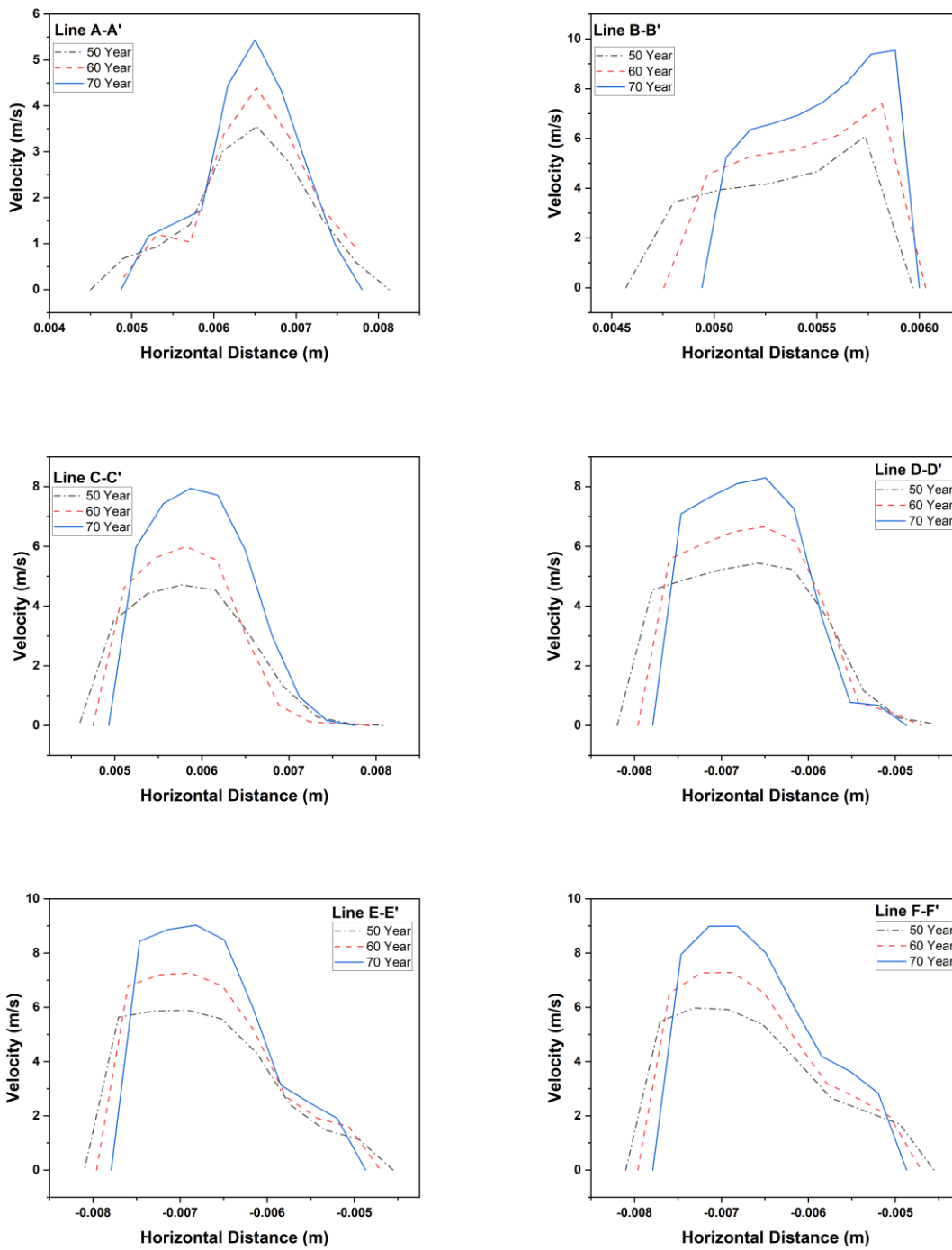
Figure 14: Comparison of the horizontal velocity of inhalation flows in the airways in relation to a developing bronchial tumor and healthy airways for each age lung model.
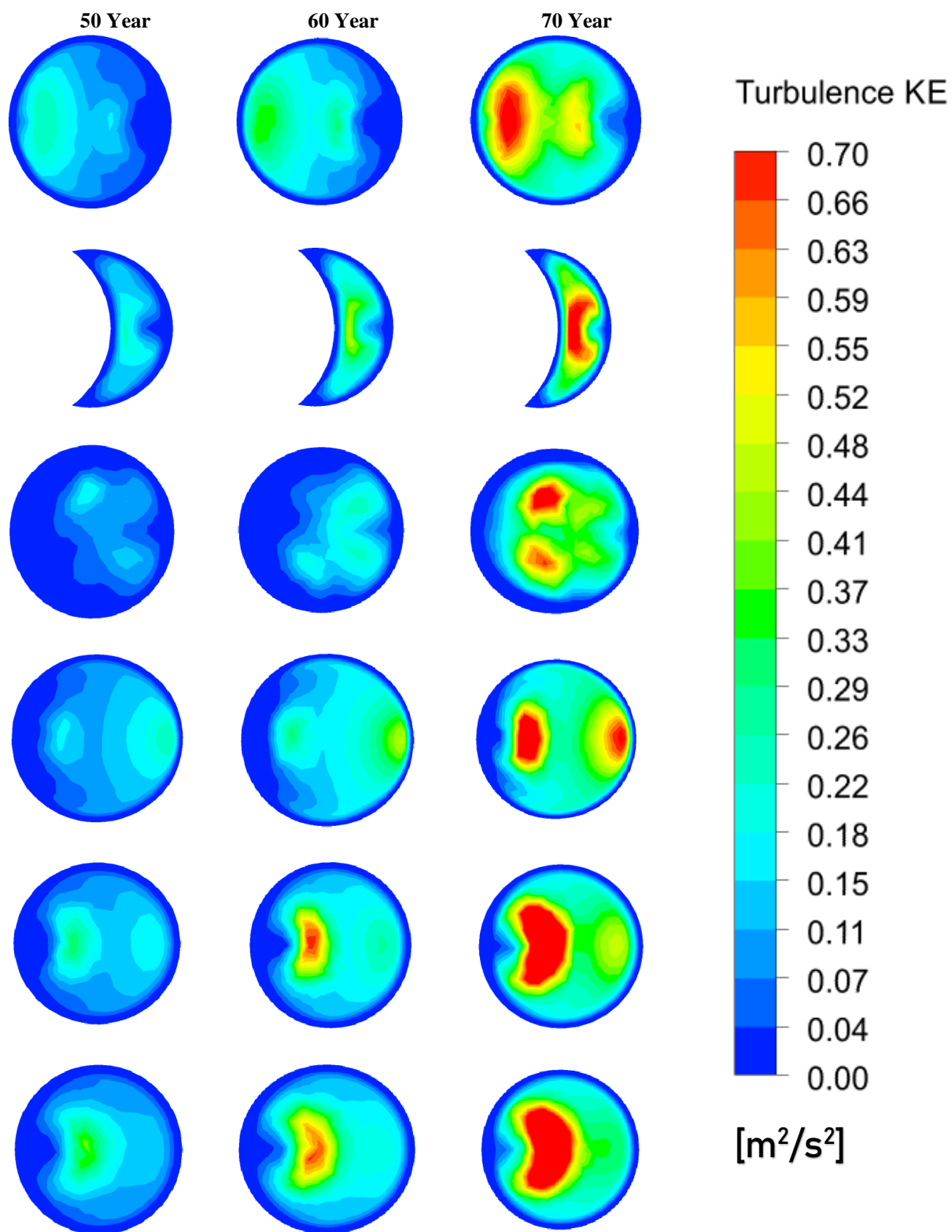
Figure 15: Turbulence Kinetic Energy at various sections of the tumor in each age model for the flow rate of 60 liter/min.

3.2   Deposition of Particles

Figure 16 shows the variation of the deposition efficiency on the tumor wall for three ages. The deposition efficiency reaches it maximum when the particle diameter is 10 µm, 12 µm and 14 µm for age 70-, 60- and 50-year-old respectively. For very small particles, the deposition efficiency is the lowest because the impact mechanism for small-sized particles becomes weak. As the flow splits at the bifurcation point, the particles with small size can alter their direction and can conveniently flow in a laminar manner which makes it easy for them to escape the higher generations and deposit in the deep bronchioles of the lung due to Brownian diffusion. For the large particle size, the impact mechanism is strong which makes the inhaled aerosols hit the boundary wall and deposit at the upper bifurcation point. These particles do not immediately follow the changes in the flow directions, and this makes it difficult for the large particles to deposit in the lower generations. For the present case, the small particles (< 10 µm) mostly escaped from the generations G3-G6 to get deposited in the lower generations whereas, the large particles (> 14 µm) got deposited mostly in the G3 and G4 before reaching the tumor wall in G5.

For particle sizes ranging from 5-10 µm , the deposition efficiency in the 50-year lung model was comparatively less due to lower inlet velocity and large surface area. The majority of these particles escaped the lung model to deposit in the deeper generations. But, for large-size particles, the maximum deposition occurred in generations G3-G6, and hence the maximum deposition on the tumor wall is found for the particle size of 14 µm in the 50-year lung model. Particles greater than 14 µm mostly got trapped in the regions above the tumor wall and hence, the deposition efficiency decreased for particles with a size greater than 14 µm. A similar trend was found for the 60-year lung model which has a maximum deposition on the tumor wall for a particle size of 12 µm. The airways in the 60-year lung model were narrower than in the 50-year lung model and the large particles with a size greater than 12 µm were more vulnerable to getting trapped in the upper generations of the lung before reaching the tumor region. Hence, the maximum deposition efficiency for the 60-year lung model was less and occurred for a lower particle size than the 50-year lung model. Compared to the 50 and 60 years old, the deposition on the tumor wall of the 70-year-old lung model was highest for the particle diameter range of 5-10 µm. The highest deposition rate for the 70-year lung model was found for the particle size of 10 µm. For particle sizes larger than 10 µm, the deposition efficiency started to decrease as the

majority of the large-size particles got deposited in the narrow airways of upper generations before reaching the tumor wall.
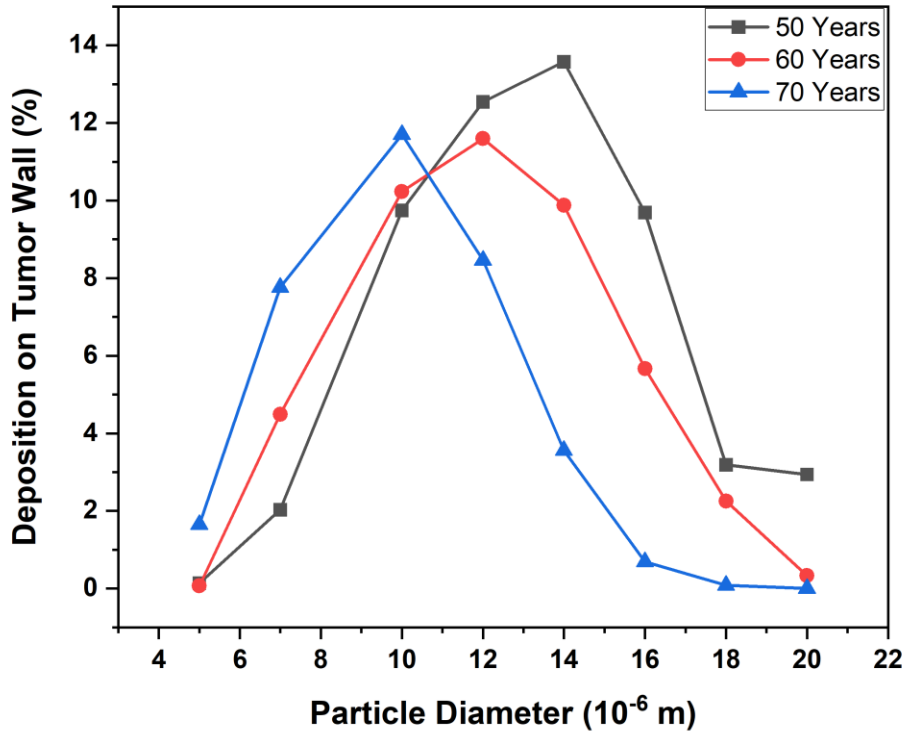
Figure 16: Deposition Efficiency on tumor wall for different ages and injected particle diameter at the flow rate of 60 liter/min.

The presence of a tumor affects the transport of the injected particles. The tumor present on the right side of G5 influences the flow of the traveling particles and diverts them toward the left side of the airway. These divergent particles then continue to move towards the left side and ultimately into the left branch or the generation following G5. Figure 17 demonstrates the comparison between the percentage of injected particles moving into the left and right branches for three different particle sizes. The number of particles traveling towards the left branch is higher than the right branch for each particle size due to the presence of the tumor.
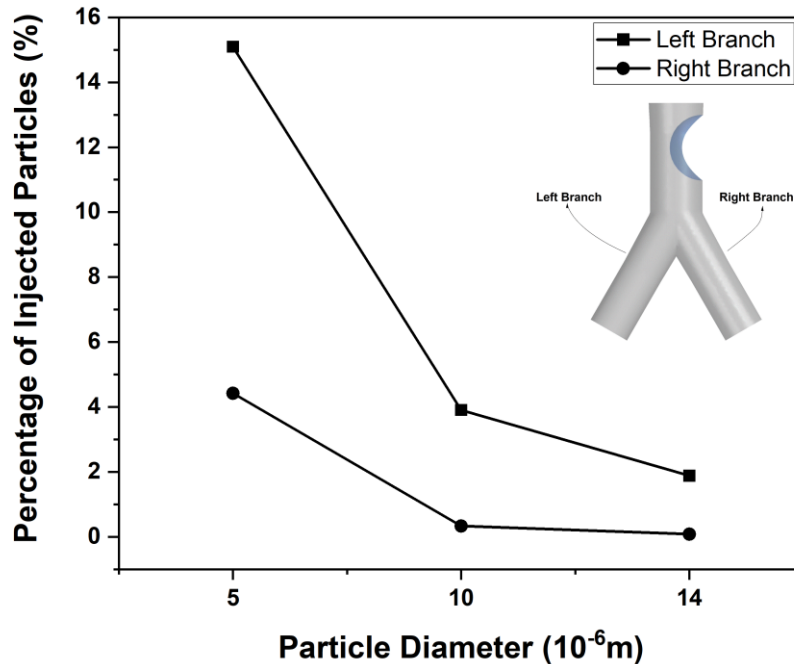
Figure 17: Comparison of number of injected particles travelling in the branches following the tumor.

Figure 18a and 18b show the deposition rate of particles in the lung surface other than the tumor and escaping rate respectively against the particle diameter. Similarly, Figure 18c and 18d shows the escaping rate and deposition efficiency of particles against the Stokes number. For small particles (5 μm), the escaping rate is 89.34%, 80.29%, and 60.39% for 50-, 60- and 70-years old lung model respectively and the corresponding deposition efficiency on the G3-G6 wall is 10.52%, 19.63%, and 37.95% respectively. This is the reason behind the low deposition of small-sized particles on the tumor wall. As the particle size increases, the deposition rate also increases, while the escape rate decreases. When dealing with large-sized particles (20 μm), the escape rate becomes almost negligible, as all of the particles are deposited on the upper generations of the lung model. Only for the particles belonging to a 10-14 μm range, the deposition on the tumor wall is considerable for each age. A similar trend of variation of deposition efficiency for small and large particle sizes is found against the Stokes number.
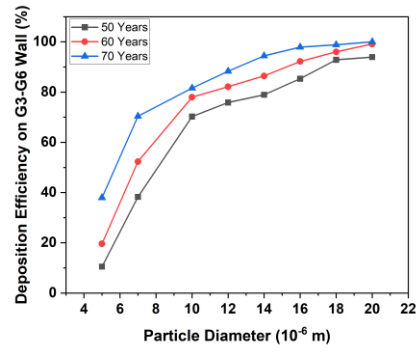
(a)
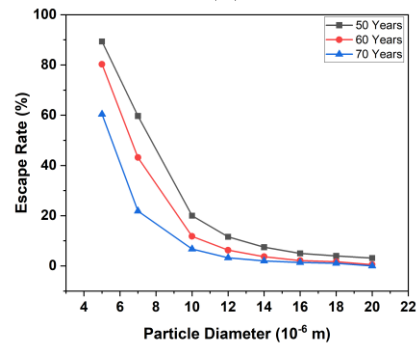
(b)
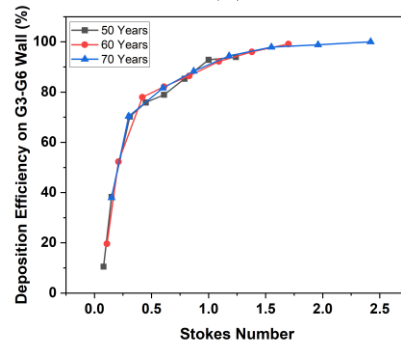
(c)
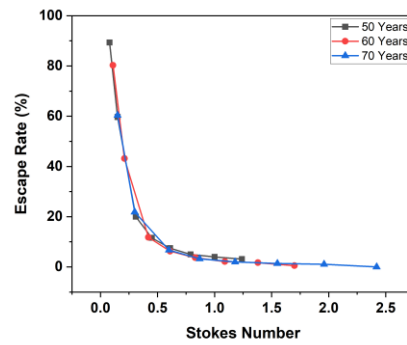
(d)

Figure 18: Deposition of particles on at the G3-G6 wall against particle diameter (a) and Stokes number (c); Escape rate for different ages against the particle diameter (b) and Stokes number (d) at the flow rate of 60 liter/min.

Figure 19 illustrates the deposition on the tumor wall against different stokes numbers and ages. The results demonstrate that due to the higher Stokes number, the majority of injected particles tend to become trapped in the walls of the upper generation. Only a small number of particles are observed to be deposited on the tumor wall specifically in generation 5 (G5). A higher Stokes number in older age also ensures that the deposition of particles on the G3-G6 lung wall of the eldest model is higher than its younger counterparts (60 and 50 years). Whereas, for the tumor wall, the maximum deposition efficiency for age 50-, 60- and 70-year-old lung models is 13.57%, 11.59%, and 11.70% respectively in the diameter range of 10-14 μm for the injected particles.
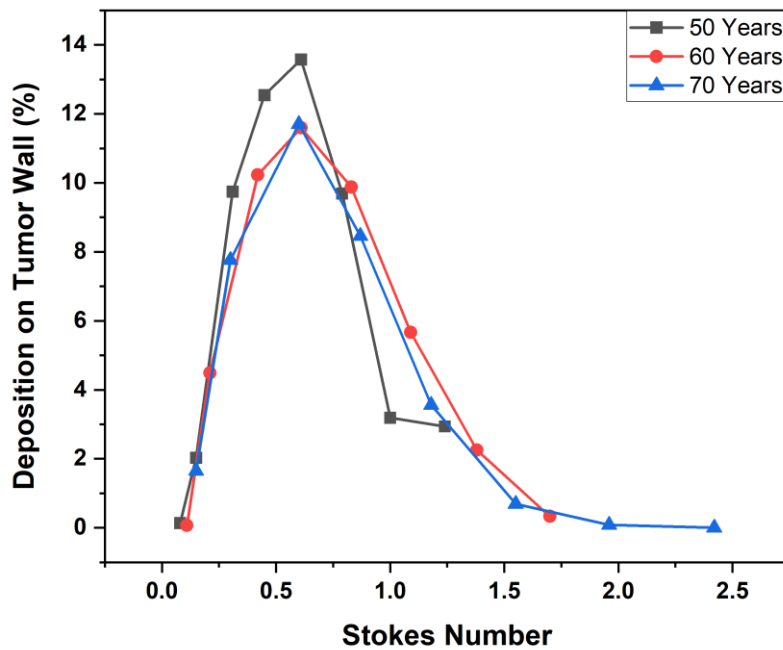
Figure 19: Variation of deposition efficiency on tumor wall with age and stokes number for the 60 liter/min flow rate.

The effect of various inhalation conditions is also investigated for a 50-year-old lung model by using three different inlet air flow rates specifically 60 liter/min, 45 liter/min, and 30 liter/min which corresponds to heavy, moderate, and light breathing respectively. The deposition efficiency on the tumor wall is maximum for a 60 liter/min flow rate followed by 45 liter/min and 30 liter/min as shown in Figure 20. The deposition efficiency on the tumor wall is less for

the small inlet flow rate because of low inertial forces and weak impact mechanism. The deposition rate increases with the high inlet flow rate. For each flow rate, the drug deposition efficiency on the tumor wall can be improved by increasing the size of the injected particle but there is a limit to this condition as well. For large and moderate inlet flow rates, particle size greater than 14 μm and 16 μm respectively causes the trapping of particles on the tumor wall to reduce significantly as majority of the particles are trapped in the higher generations before reaching the tumor wall.
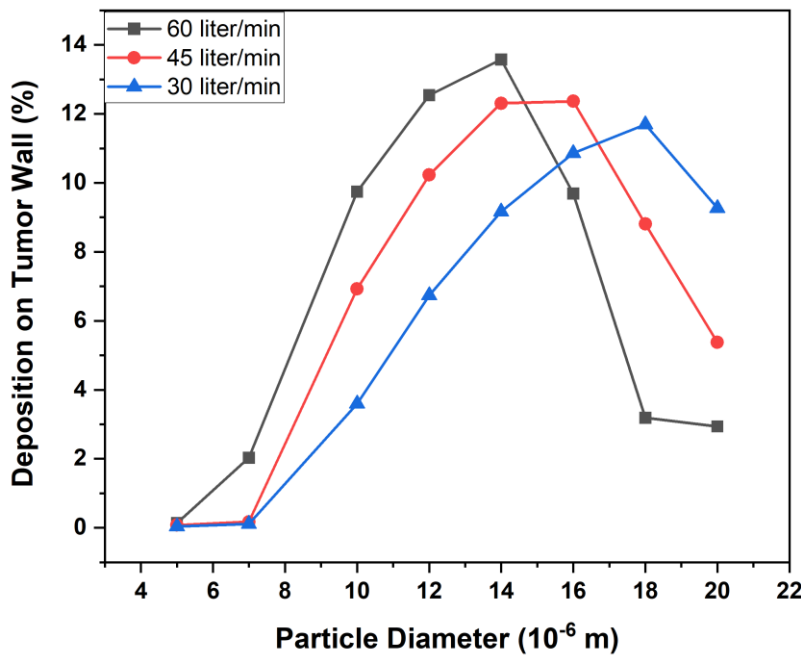
Figure 20: Deposition Efficiency on tumor wall for different inlet flow rates and injected particle diameter for the 50-year-old lung model.

For small inlet flow rate, the particle deposition for a large particle size ($18 \mu m$) is well higher than the small-sized particles but still lower than the other inlet flow rates. This is because due to the small velocity and approximately streamlined flow for small inlet flow rate, particles tend to move along straight path lines and travel through the upper generations without depositing and trapping deeper into the lungs such as on the tumor wall present in G5. The maximum deposition efficiency on the tumor wall was 13.57%, 12.36%, and 11.69% for large, moderate, and small inlet flow rates respectively. Also, the particle deposition on the lung walls is higher for large inlet flow rate as depicted in Figure 21a. The escape rate for small inlet flow

rate is higher as compared to moderate and large flow rates (see Figure 21b). This is because high inertial forces during large flow rate cause the particles to trap on lung wall and tumor surface which leaves behind a smaller number of particles that can escape into the lower generations especially the particles with large diameters. Based on the calculated patterns of drug deposition on the tumor wall, the patient is advised to inhale the drugs at a high flow rate for maximum deposition of particles on the targeted lung region. Moreover, the optimal size for the injected particles is dependent on the targeted location.
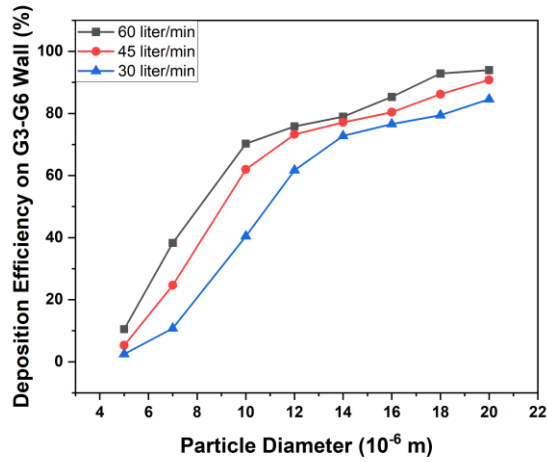
(a)
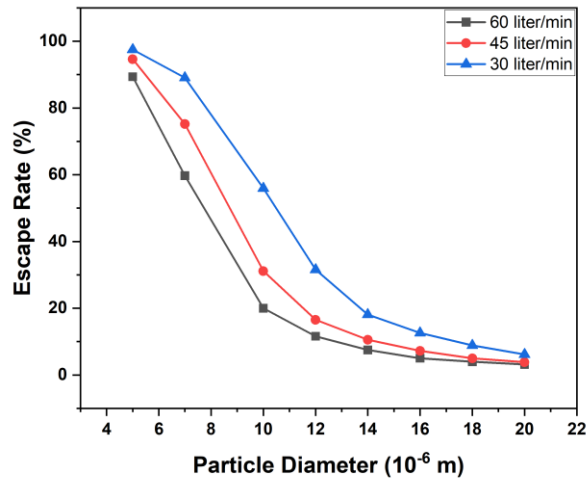
(b)

Figure 21: Deposition of particles on the G3-G6 wall (a) and escape rate (b) for different flow rates and diameter sizes for 50-year-old lung model.
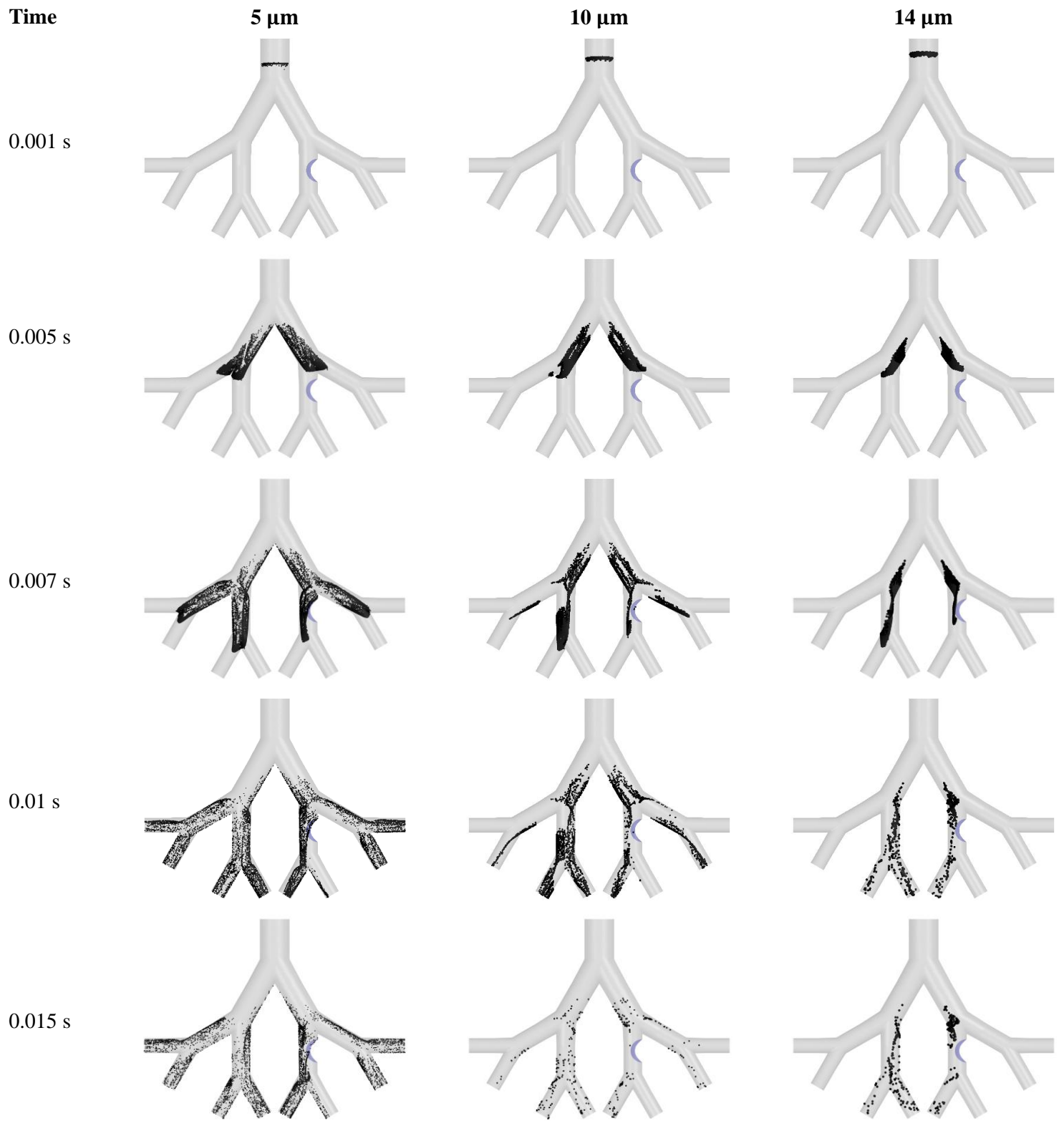
Figure 22: Particle transport in the 50-year lung model for particle size of 5μm, 10μm and 14μm at the flow rate of 60 liter/min.

Figure 22 illustrates the transport of particles with sizes 5 µm, 10 µm, and 14 µm in the 50-year lung model for the inlet flow rate of 60 liter/min. The particle transport is demonstrated at different timesteps to visualise the location and flow behaviour of particles through the G3-G6 lung model. Figure 22 illustrates that for particles with a size of 5 µm, a higher concentration is observed within the lung model domain. This higher concentration indicates a lower deposition efficiency on the G3-G6 airway generations and the tumor wall. Whereas the deposition of particles with a size of 14 µm is the maximum for the 50-year lung model which can be indicated by the low concentration of particles in the domain of the lung model for the particle size of 14 µm. For the present study, the optimal size is found to be in the range of 10-14 µm for maximum effectiveness of the inhaled drug. Also, small-sized particles move into the deeper airways whereas the large-sized particles just deposit even before reaching the targeted region for each inlet flow rate.

CHAPTER 4

CONCLUSION

The TD of micro-scale particles in the tracheobronchial airway generations G3-G6 of an unhealthy lung with a presence of a sidewall tumor for three sets of ages and three inlet air flow rates are investigated. Wall shear stress, velocity contours at different cross-sectional planes, and pressure contours are compared for each lung model and the main findings from the study are summarised below:

- As the age increased, the airflow velocity on the tumor wall also increased due to changes in the geometrical parameters of the lung and a reduction in the cross-sectional area. The shear stress on the tumor wall and pressure drop also increased with age due to the high impact mechanism and velocity gradient. The velocity, wall shear, and pressure drop also increased with the inlet flow rate for each age. Due to increased velocity magnitudes and impact mechanism for older age, the particle deposition on the G3-G6 lung wall for the 70-year-old lung is maximum when compared with other models. Moreover, for the tumor wall, eldest lung has the highest deposition efficiency for the particle size up to 10 µm and for the particle size ranging between 10 µm-20 µm, the highest deposition efficiency is observed for the 50-year-old lung.

- The presence of a tumor can significantly alter the trajectory of incoming particles, resulting in a diversion toward the opposite side of the airway. Consequently, a non-uniform distribution of particles occurs in the generation following the obstructed airway, leading to one branch receiving a lower particle count than the other.

- The deposition of particles on the tumor wall depends greatly on the size of the injected particles. Particles with 10 µm-14 µm diameter have maximum deposition on the tumor wall located in the 5th generation for each age, whereas particles with a size less than 10 µm mostly escape the G3-G6 lung region and are deposited into the deeper airways. For particles larger than 14 µm, the deposition efficiency is found to be higher in the upper generations of the lung, with only a small number of injected particles reaching the tumor wall. Furthermore, it is observed that the variation trends of deposition efficiency differ between the tumor wall and the G3-G6 lung wall with respect to particle size. Hence, depending on

the location of the targeted region inside an age-specific lung, the size of the injected particle can be adjusted for optimal delivery and treatment.

- The deposition efficiency is significantly influenced by the inlet flow rate. More particles are deposited on the tumor wall for large inlet flow rate as compared to particles of the same size for medium and small inlet flow rates for the same age.

- Moreover, for small inlet flow rate, particles with large diameters tend to move deeper into the airways as compared to the large inlet flow rate. Hence for large flow rate, particle size ranging between 10 µm-14 µm, and for small inlet flow rate, particle size ranging between 12 µm -18 µm is optimal for treating the growth of a glomus tumor in the upper tracheobronchial airways.

One of the limitations of this study is the utilization of an idealized airway model instead of a patient-specific model for validation purposes. Although an idealized model provides a useful framework for comprehending the general airflow patterns and particle dynamics in the lung airways, it may not fully capture the individual variations and complexities present in real patients. The lack of patient-specific data restricts the ability to assess the accuracy and applicability of the findings to diverse populations with unique airway geometries. Therefore, future studies incorporating personalized airway models are essential to enhance the reliability and clinical relevance of the research outcomes. Open outlet and uniform pressure are used at the outlet: Another limitation of this study is the assumption of an open outlet with uniform pressure at the airway's exit. While this simplification allows for easier computational modeling and analysis, it does not accurately represent the physiological conditions of the respiratory system. In reality, the lungs have a complex branching structure with varying diameters and compliance, and the presence of anatomical features such as alveoli and bronchioles significantly affects airflow dynamics. Additionally, the use of a uniform pressure boundary condition may oversimplify the natural pressure gradients that exist throughout the respiratory system. It is important to note that this study solely focused on the analysis of particle transport and deposition during inhalation. While inhalation plays a crucial role in assessing the entry of aerosol particles into the respiratory system, it neglects the equally significant process of exhalation. Exhalation influences the clearance of particles from the airways, as well as their deposition patterns. Therefore, by excluding the exhalation phase, this study provides an incomplete understanding of the overall particle dynamics within the lung airways. Future

investigations that encompass both inhalation and exhalation phases would yield more comprehensive insights into the behavior of particles throughout the entire respiratory cycle, contributing to a more accurate evaluation of their deposition patterns and potential health effects.

However, despite these limitations, it is worth noting that previous studies have demonstrated that the utilization of a symmetric and planar lung airways model can still provide accurate predictions of particle deposition patterns. Hence, despite the limitations mentioned earlier, the observed airflow characteristics and particle deposition patterns in our study are still valid and in line with the findings reported in the existing published literature. The present study critically analyzed the flow behavior in a tumorous lung, aiming to understand its implications for human health and well-being. Comprehensive qualitative and quantitative analysis of the velocity magnitude, pressure drop, and wall shear would help to understand the breathing dynamics of cancer patients. The detailed analysis of aerosol transport dynamics through the tumorous section of the airways improves the knowledge of the field and helps the development of future therapeutics. The findings of the present study would be beneficial for enhancing the quality of drug delivery through inhaling equipment and for better treatment of pulmonary diseases.

REFERENCES

[1]   C. Kleinstreuer and Z. Zhang, "Targeted drug aeroso deposition analysis for a four-generation lung airway model with hemispherical tumors," *Journal of Biomechanical Engineering,* vol. 125, no. 2, pp. 197-206, 2003.

[2]   A. J. Cohen, "Outdoor air pollution and lung cancer," *Environmental health perspectives,* vol. 108, no. suppl 4, pp. 743-750, 2000.

[3]   N. Akhtar and J. G. Bansal, "Risk factors of Lung Cancer in nonsmoker," *Current problems in cancer,* vol. 41, no. 5, pp. 328-339, 2017.

[4]   A. J. Alberg and J. M. Samet, "Epidemiology of lung cancer," *Chest,* vol. 123, no. 1, pp. 21S-49S, 2003.

[5]   W. Hohenforst-Schmidt *et al.*, "Glomus tumor in the lung parenchyma," *Journal of thoracic disease,* vol. 4, no. 6, p. 663, 2012.

[6]   H. Sung *et al.*, "Global cancer statistics 2020: GLOBOCAN estimates of incidence and mortality worldwide for 36 cancers in 185 countries," *CA: a cancer journal for clinicians,* vol. 71, no. 3, pp. 209-249, 2021.

[7]   R. F. Oliveira, S. F. Teixeira, L. F. Silva, J. C. Teixeira, and H. Antunes, "Development of new spacer device geometry: a CFD study (part I)," *Computer methods in biomechanics biomedical engineering,* vol. 15, no. 8, pp. 825-833, 2012.

[8]   J. M. Borghardt, C. Kloft, and A. Sharma, "Inhaled therapy in respiratory disease: the complex interplay of pulmonary kinetic processes," *Canadian respiratory journal,* vol. 2018, 2018.

[9]   M. Rahman, M. Zhao, M. S. Islam, K. Dong, and S. C. Saha, "Numerical study of nano and micro pollutant particle transport and deposition in realistic human lung airways," *Powder Technology,* vol. 402, p. 117364, 2022.

[10]   K. L. Parker, M. D. Zervos, J. S. Donington, P. S. Shukla, and C. S. Bizekis, "Tracheal glomangioma in a patient with asthma and chest pain," *Journal of Clinical Oncology,* vol. 28, no. 2, pp. e9-e10, 2010.

[11]   F. Colaut, L. Toniolo, A. Scapinello, and M. Pozzobon, "Tracheal glomus tumor successfully resected with rigid bronchoscopy: a case report," *Journal of Thoracic Oncology,* vol. 3, no. 9, pp. 1065-1067, 2008.

[12] Y. Shang *et al.*, "Removal of glomus tumor in the lower tracheal segment with a flexible bronchoscope: report of two cases," *Internal Medicine,* vol. 49, no. 9, pp. 865-869, 2010.

[13] M. Watanabe *et al.*, "Successful resection of a glomus tumor arising from the lower trachea: report of a case," *Surgery today,* vol. 28, no. 3, pp. 332-334, 1998.

[14] J. Valerian Corda, J. Emmanuel, S. Nambiar, and M. Zuber, "Airflow patterns and particle deposition in a pediatric nasal upper airway following a rapid maxillary expansion: Computational fluid dynamics study," *Cogent Engineering,* vol. 10, no. 1, p. 2158614, 2023.

[15] K. Inthavong, Y. Ye, S. Ding, and J. Tu, "Comparative study of the effects of acute asthma in relation to a recovered airway tree on airflow patterns," in *13th International Conference on Biomedical Engineering: ICBME 2008 3–6 December 2008 Singapore*, 2009: Springer, pp. 1555-1558.

[16] F. Huang *et al.*, "Role of CFD based in silico modelling in establishing an in vitro-in vivo correlation of aerosol deposition in the respiratory tract," *Advanced Drug Delivery Reviews,* vol. 170, pp. 369-385, 2021.

[17] T. Gemci, V. Ponyavin, R. Collins, T. E. Corcoran, S. C. Saha, and M. S. Islam, "CFD study of dry pulmonary surfactant aerosols deposition in upper 17 generations of human respiratory tract," *Atmosphere,* vol. 13, no. 5, p. 726, 2022.

[18] M. S. Islam *et al.*, "How severe acute respiratory syndrome coronavirus-2 aerosol propagates through the age-specific upper airways," *Physics of Fluids,* vol. 33, no. 8, p. 081911, 2021.

[19] X. April Si, M. Talaat, and J. Xi, "SARS COV-2 virus-laden droplets coughed from deep lungs: Numerical quantification in a single-path whole respiratory tract geometry," *Physics of Fluids,* vol. 33, no. 2, p. 023306, 2021.

[20] Á. Farkas, P. Füri, W. Thén, and I. Salma, "Effects of hygroscopic growth of ambient urban aerosol particles on their modelled regional and local deposition in healthy and COPD-compromised human respiratory system," *Science of the Total Environment,* vol. 806, p. 151202, 2022.

[21] M. H. Taheri, O. Pourmehran, M. M. Sarafraz, K. Ahookhosh, A. Farnoud, and X. Cui, "Effect of swirling flow and particle-release pattern on drug delivery to human

tracheobronchial airways," *Biomechanics and Modeling in Mechanobiology,* vol. 20, pp. 2451-2469, 2021.

[22]   Y. Jin, H. Cui, L. Chen, K. Sun, and Z. Liu, "Effects of airway deformation and alveolar pores on particle deposition in the lungs," *Science of the Total Environment,* vol. 831, p. 154931, 2022.

[23]   C. Ou, J. Hang, and Q. Deng, "Particle deposition in human lung airways: effects of airflow, particle size, and mechanisms," *Aerosol and Air Quality Research,* vol. 20, no. 12, pp. 2846-2858, 2020.

[24]   E. R. Weibel, A. F. Cournand, and D. W. Richards, *Morphometry of the human lung*. Springer, 1963.

[25]   M. M. Rahman, M. Zhao, M. S. Islam, K. Dong, and S. C. Saha, "Aging effects on airflow distribution and micron-particle transport and deposition in a human lung using CFD-DPM approach," *Advanced Powder Technology,* vol. 32, no. 10, pp. 3506-3516, 2021.

[26]   G. Xu and C. Yu, "Effects of age on deposition of inhaled aerosols in the human lung," *Aerosol Science and Technology,* vol. 5, no. 3, pp. 349-357, 1986.

[27]   B. Asgharian, M. Menache, and F. Miller, "Modeling age-related particle deposition in humans," *Journal of Aerosol Medicine,* vol. 17, no. 3, pp. 213-224, 2004.

[28]   R. F. Patterson, Q. Zhang, M. Zheng, and Y. Zhu, "Particle deposition in respiratory tracts of school-aged children," *Aerosol and Air Quality Research,* vol. 14, no. 1, pp. 64-73, 2014.

[29]   F. Hrubá, E. Fabiánová, K. Koppová, and J. J. Vandenberg, "Childhood respiratory symptoms, hospital admissions, and long-term exposure to airborne particulate matter," *Journal of Exposure Analysis and Environmental Epidemiology,* vol. 11, no. 1, pp. 33-40, 2001.

[30]   J. Huang and L. Zhang, "Micro-particle deposition and lobar distribution of mass flow in human upper respiratory tract model," *Chinese Science Bulletin,* vol. 56, no. 4, pp. 380-385, 2011.

[31]   R. Segal, X. Guan, M. Shearer, and T. Martonen, "Mathematical model of airflow in the lungs of children I; effects of tumor sizes and locations," *Computational Mathematical Methods in Medicine,* vol. 2, no. 3, pp. 199-213, 2000.

[32] X. Yang, Y. Liu, and H. Luo, "Respiratory flow in obstructed airways," *Journal of Biomechanics,* vol. 39, no. 15, pp. 2743-2751, 2006.

[33] B. Sul, A. Wallqvist, M. J. Morris, J. Reifman, and V. Rakesh, "A computational study of the respiratory airflow characteristics in normal and obstructed human airways," *Computers in Biology and Medicine,* vol. 52, pp. 130-143, 2014.

[34] T. B. Martonen and X. Guan, "Effects of tumors on inhaled pharmacologic drugs: I. Flow patterns," *Cell Biochem Biophys,* 2001, doi: 10.1385/CBB:35:3:233.

[35] T. B. Martonen and X. Guan, "Effects of Tumors on Inhaled Pharmacologic Drugs: II. Particle Motion," *Cell Biochemistry and Biophysics,* vol. 35, 2001.

[36] H. Luo, Y. Liu, and X. Yang, "Particle deposition in obstructed airways," *Journal of Biomechanics,* vol. 40, no. 14, pp. 3096-3104, 2007.

[37] V. Srivastav, A. Kumar, S. Shukla, A. Paul, A. Bhatt, and A. Jain, "Airflow and aerosol-drug delivery in a CT scan based human respiratory tract with tumor using CFD," *Journal of Applied Fluid Mechanics,* vol. 7, no. 2, pp. 345-356, 2014.

[38] D. Singh, "Numerical assessment of natural respiration and particles deposition in the computed tomography scan airway with a glomus tumour," *Proceedings of the Institution of Mechanical Engineers, Part E: Journal of Process Mechanical Engineering,* vol. 235, no. 6, pp. 1945-1956, 2021.

[39] Y. M. Menaissy, A. A. Gal, and K. A. Mansour, "Glomus tumor of the trachea," *The Annals of Thoracic Surgery,* vol. 70, no. 1, pp. 295-297, 2000.

[40] K. Fukumitsu *et al.*, "Tracheal Glomus Tumor Complicated with Asthma Exacerbation in a Pregnant Woman," *Internal Medicine,* pp. 0510-22, 2023.

[41] J.-F. Daisne *et al.*, "Tumor volume in pharyngolaryngeal squamous cell carcinoma: comparison at CT, MR imaging, and FDG PET and validation with surgical specimen," *Radiology,* vol. 233, no. 1, pp. 93-100, 2004.

[42] K. C. Thandra, A. Barsouk, K. Saginala, J. S. Aluru, and A. Barsouk, "Epidemiology of lung cancer," *Contemporary Oncology/Współczesna Onkologia,* vol. 25, no. 1, pp. 45-52, 2021.

[43] J. D. Mitchell *et al.*, "Resection for bronchogenic carcinoma involving the carina: long-term results and effect of nodal status on outcome," *The Journal of Thoracic Cardiovascular Surgery,* vol. 121, no. 3, pp. 465-471, 2001.

[44]   W. Hofmann, "Mathematical model for the postnatal growth of the human lung," *Respiration physiology,* vol. 49, no. 1, pp. 115-129, 1982.

[45]   J. Kim, R. L. Heise, A. M. Reynolds, and R. M. Pidaparti, "Aging effects on airflow dynamics and lung function in human bronchioles," *PloS one,* vol. 12, no. 8, p. e0183654, 2017.

[46]   S. J. Lai-Fook and R. E. Hyatt, "Effects of age on elastic moduli of human lungs," *Journal of Applied Physiology,* vol. 89, no. 1, pp. 163-168, 2000.

[47]   K. Oho and R. Amemiya, *Practical Fiberoptic Bronchoscopy* Igaku-Shoin, 1980.

[48]   J. Xi, J. Kim, X. A. Si, R. A. Corley, S. Kabilan, and S. Wang, "CFD modeling and image analysis of exhaled aerosols due to a growing bronchial tumor: towards non-invasive diagnosis and treatment of respiratory obstructive diseases," *Theranostics,* vol. 5, no. 5, p. 443, 2015.

[49]   E. Y. Park *et al.*, "Impact of environmental exposure to persistent organic pollutants on lung cancer risk," *Environment International,* vol. 143, p. 105925, 2020.

[50]   F. R. Menter, "Improved two-equation k-omega turbulence models for aerodynamic flows," 1992.

[51]   A. Tiwari, A. Jain, A. R. Paul, and S. C. Saha, "Computational evaluation of drug delivery in human respiratory tract under realistic inhalation," *Physics of Fluids,* vol. 33, no. 8, p. 083311, 2021.

[52]   M. Sommerfeld, O. Sgrott Jr, M. Taborda, P. Koullapis, K. Bauer, and S. Kassinos, "Analysis of flow field and turbulence predictions in a lung model applying RANS and implications for particle deposition," *European Journal of Pharmaceutical Sciences,* vol. 166, p. 105959, 2021.

[53]   J. Wedel, P. Steinmann, M. Štrakl, M. Hriberšek, and J. Ravnik, "Can CFD establish a connection to a milder COVID-19 disease in younger people? Aerosol deposition in lungs of different age groups based on Lagrangian particle tracking in turbulent flow," *Computational Mechanics,* vol. 67, no. 5, pp. 1497-1513, 2021.

[54]   Z. Zhang and C. Kleinstreuer, "Laminar-to-turbulent fluid–nanoparticle dynamics simulations: Model comparisons and nanoparticle-deposition applications," *International Journal for Numerical Methods in Biomedical Engineering,* vol. 27, no. 12, pp. 1930-1950, 2011.

[55] M. S. Islam, G. Paul, H. X. Ong, P. M. Young, Y. Gu, and S. C. Saha, "A review of respiratory anatomical development, air flow characterization and particle deposition," *International Journal of Environmental Research Public Health,* vol. 17, no. 2, p. 380, 2020.

[56] M. M. Rahman, M. Zhao, M. S. Islam, K. Dong, and S. C. Saha, "Aerosol Particle Transport and Deposition in Upper and Lower Airways of Infant, Child and Adult Human Lungs," *Atmosphere,* vol. 12, no. 11, p. 1402, 2021.

[57] M. S. Islam, S. C. Saha, E. Sauret, H. Ong, P. Young, and Y. Gu, "Euler–Lagrange approach to investigate respiratory anatomical shape effects on aerosol particle transport and deposition," *Toxicology Research Application,* vol. 3, p. 2397847319894675, 2019.

[58] M. Rahimi-Gorji, O. Pourmehran, M. Gorji-Bandpy, and T. Gorji, "CFD simulation of airflow behavior and particle transport and deposition in different breathing conditions through the realistic model of human airways," *Journal of Molecular Liquids,* vol. 209, pp. 121-133, 2015.

[59] M. S. Islam, Y. Gu, A. Farkas, G. Paul, and S. C. Saha, "Helium–oxygen mixture model for particle transport in CT-based upper airways," *International journal of environmental research public health,* vol. 17, no. 10, p. 3574, 2020.

[60] W. Zhang, Y. Xiang, C. Lu, C. Ou, and Q. Deng, "Numerical modeling of particle deposition in the conducting airways of asthmatic children," *Medical Engineering Physics,* vol. 76, pp. 40-46, 2020.

[61] A. Arsalanloo, M. Abbasalizadeh, M. Khalilian, Y. Saniee, A. Ramezanpour, and M. S. Islam, "A computational approach to understand the breathing dynamics and pharmaceutical aerosol transport in a realistic airways," *Advanced Powder Technology,* vol. 33, no. 7, p. 103635, 2022.

[62] C. S. Kim and D. M. Fisher, "Deposition characteristics of aerosol particles in sequentially bifurcating airway models," *Aerosol Science Technology,* vol. 31, no. 2-3, pp. 198-220, 1999.

[63] Y. Feng and C. Kleinstreuer, "Micron-particle transport, interactions and deposition in triple lung-airway bifurcations using a novel modeling approach," *Journal of Aerosol Science,* vol. 71, pp. 1-15, 2014.

[64]   X. Chen, W. Zhong, X. Zhou, B. Jin, and B. Sun, "CFD–DEM simulation of particle transport and deposition in pulmonary airway," *Powder technology,* vol. 228, pp. 309-318, 2012.

[65]   M. J. Rhodes, *Introduction to particle technology*. John Wiley & Sons, 2008.